Eur. Phys. J. C 52, 141–158 (2007)
DOI 10.1140/epjc/s10052-007-0359-7

THE EUROPEAN PHYSICAL JOURNAL C

Regular Article – Theoretical Physics

Low-energy $\pi\pi$ and πK scatterings revisited in three-flavour resummed chiral perturbation theory

S. Descotes-Genon[a]

Laboratoire de Physique Théorique, CNRS/Univ. Paris-Sud 11 (UMR 8627), 91405 Orsay Cedex, France

Received: 31 March 2007 / Revised version: 25 May 2007 /
Published online: 19 July 2007 –

Abstract. Chiral symmetry breaking may exhibit significantly different patterns in two chiral limits: $N_f = 2$ massless flavours ($m_u = m_d = 0$, m_s physical) and $N_f = 3$ massless flavours ($m_u = m_d = m_s = 0$). Such a difference may arise due to vacuum fluctuations of $s\bar{s}$ pairs related to the violation of the Zweig rule in the scalar sector, and it could yield numerical competition between contributions counted as leading and next-to-leading order in the chiral expansions of the observables. We recall and extend resummed chiral perturbation theory (ReχPT), a framework that we introduced previously to deal with such instabilities: it requires a more careful definition of the relevant observables and their one-loop chiral expansions. We analyse the amplitudes for low-energy $\pi\pi$ and πK scatterings within ReχPT, which we match in subthreshold regions with dispersive representations obtained from the solutions of the Roy and Roy–Steiner equations. Using a frequentist approach, we constrain the quark mass ratio as well as the quark condensate and the pseudoscalar decay constant in the $N_f = 3$ chiral limit. The results mildly favour significant contributions of vacuum fluctuations suppressing the $N_f = 3$ quark condensate compared to its $N_f = 2$ counterpart.

1 Introduction

A striking feature of the standard model consists in the mass hierarchy obeyed by the light quarks:

$$m_u \sim m_d \ll m_s \sim \Lambda_{\rm QCD} \ll \Lambda_{\rm H}\,, \tag{1}$$

where $\Lambda_{\rm QCD}$ is the characteristic scale describing the running of the QCD effective coupling and $\Lambda_{\rm H} \sim 1\,{\rm GeV}$ the mass scale of the bound states not protected by chiral symmetry. Therefore, the strange quark may play a special role in the low-energy dynamics of QCD:

(i) it is light enough to allow for a combined expansion of observables in powers of m_u, m_d, m_s around the $N_f = 3$ chiral limit (meaning three massless flavours):

$$N_f = 3: \quad m_u = m_d = m_s = 0\,; \tag{2}$$

(ii) it is sufficiently heavy to induce significant changes in order parameters from the $N_f = 3$ chiral limit to the $N_f = 2$ chiral limit (meaning two massless flavours):

$$N_f = 2: \quad m_u = m_d = 0 \quad m_s \text{ physical}\,; \tag{3}$$

(iii) it is too light to suppress efficiently loop effects of massive $\bar{s}s$ pairs (contrary to c, b, t quarks).

These three arguments suggest that $\bar{s}s$ sea pairs may play a significant role in chiral dynamics, leading to different patterns of chiral symmetry breaking in the $N_f = 2$ and $N_f = 3$ chiral limits. Then, chiral order parameters such as the quark condensate and the pseudoscalar decay constant,

$$\Sigma(N_f) = -\lim_{N_f} \langle \bar{u}u \rangle\,, \quad F^2(N_f) = \lim_{N_f} F_\pi^2\,, \tag{4}$$

would have significantly different values in the two chiral limits ($\lim_{N_f}$ denoting the chiral limit with N_f massless flavours).

The role of $\bar{s}s$ pairs in the structure of QCD vacuum is a typical loop effect: it should be suppressed in the large-N_c limit, and it can be significant only if the Zweig rule is badly violated in the vacuum (scalar) channel $J^{PC} = 0^{++}$. On general theoretical grounds [1], one expects $\bar{s}s$ sea-quark pairs to have a paramagnetic effect on the chiral order parameters, so that they should decrease when the strange quark mass is sent to zero: for instance, $\Sigma(2; m_s) \geq \Sigma(2; m_s = 0)$, and similarly for F^2, which translates into the paramagnetic inequalities:

$$\Sigma(2) \geq \Sigma(3)\,, \quad F^2(2) \geq F^2(3)\,. \tag{5}$$

However, the size of this paramagnetic suppression is not predicted. Thus, it is highly desirable to extract the size of the chiral order parameters in $N_f = 2$ and $N_f = 3$ limits from experiment.

Recent data on $\pi\pi$ scattering [2,3] together with older data and numerical solutions of the Roy equations [4] allowed us to determine the $N_f = 2$ order parameters ex-

[a] e-mail: descotes@th.u-psud.fr

pressed in suitable physical units [5]:

$$X(2) = \frac{(m_u + m_d)\Sigma(2)}{F_\pi^2 M_\pi^2} = 0.81 \pm 0.07\,, \tag{6}$$

$$Z(2) = \frac{F^2(2)}{F_\pi^2} = 0.89 \pm 0.03\,. \tag{7}$$

A different analysis of the data in [2, 3] with the additional input of dispersive estimates for the (non-strange) scalar radius of the pion led to a larger value of $X(2)$ [6]. $X(2)$ and $Z(2)$ seem to be fairly close to 1, so that corrections related to $m_u, m_d \neq 0$ (while m_s remains at its physical value) have a limited impact on the low-energy behaviour of QCD. In turn, two-flavour chiral perturbation theory (χPT) [7], which consists in an expansion in powers of m_u and m_d around the $N_f = 2$ chiral limit, would not suffer from severe problems of convergence.[1]

Two-flavour χPT [7] deals only with dynamical pions in a very limited range of energy. In order to include K- and η-mesons dynamically and extend the energy range of interest, one must use three-flavour χPT [13] in which the expansion in the three light-quark masses starts around the $N_f = 3$ vacuum $m_u = m_d = m_s = 0$. From the above discussion, large vacuum fluctuations of $\bar{s}s$ pairs would have a dramatic effect on $N_f = 3$ chiral expansions. The leading-order (LO) term, which depends on the $O(p^2)$ low-energy constants $F^2(3)$ and $\Sigma(3)$, would be damped. On the other hand, next-to-leading-order (NLO) corrections could be enhanced, in particular those related to Zweig rule violation in the scalar sector. For instance, the Gell-Mann–Oakes–Renner relation would not be saturated by its LO term and would receive sizable numerical contributions from terms counted as NLO in the chiral counting.

Unfortunately, the experimental data on K and η decays are not accurate enough to assess the role of $s\bar{s}$ pairs in the N_f-dependence of chiral symmetry breaking in a very precise way. However our understanding of πK scattering at low energies has been improved recently through the re-analysis of the dispersive Roy–Steiner equations [14]. A rapid analysis of its results in the framework of three-flavour χPT hinted at significant vacuum fluctuations encoded in some $O(p^4)$ chiral couplings, which calls for a more detailed analysis of the πK system. Interesting information can also be obtained from our current knowledge of $\pi\pi$ scattering, which we will include in our study.

To perform such an analysis, we develop and modify the framework presented in [1, 15, 16]. Specifically, our work differs from [16] on three points: we consider not only $\pi\pi$ but also πK scattering; our observables are the values of the amplitudes in unphysical regions rather than subtraction constants of dispersion relations, and the matching between theoretical and experimental representations is performed in a frequentist approach, not in a Bayesian framework.

In Sect. 2, we motivate and explain resummed chiral perturbation theory (ReχPT), a framework designed to derive three-flavour chiral series at one loop, in which vacuum fluctuations of $s\bar{s}$ pairs are resummed. In Sect. 3, we apply ReχPT to $\pi\pi$ and πK scattering amplitudes and we explain how we determine the same amplitudes dispersively in subthreshold regions, building upon the solutions of the Roy and Roy–Steiner equations [4, 14]. In Sect. 4, we discuss the matching of the chiral and dispersive results within a frequentist approach [17], and in Sect. 5 we present our results for the order parameters of $N_f = 3$ chiral symmetry breaking. In Sect. 6, we summarise and discuss our results. The appendices are devoted to the expression of the scattering amplitudes in ReχPT, their evaluation from the Roy and Roy–Steiner equations and the treatment of correlated data.

2 Resummed chiral perturbation theory

We start by describing in more detail the framework introduced in [1, 15, 16] to expand the observables around the $N_f = 3$ chiral limit in the case of significant vacuum fluctuations. We take this opportunity to extend this framework to deal with energy-dependent quantities.

2.1 Convergence of observables

In the introduction, we emphasised the possibility for a three-flavour chiral series to exhibit a rather unusual behaviour, with numerical competition between leading and next-to-leading order. In [16], we called such a numerical competition between terms of different chiral counting instability of the expansion. A naïve argument based on resonance saturation suggests that higher orders in the chiral expansion should be suppressed by powers of $(F_\pi/\Lambda_{\rm H})^2$. However, such an argument does not apply to a leading-order contribution proportional to $\Sigma(3)$ [20–22]: there is no resonance that could saturate the quark condensate. Therefore we expect to encounter three-flavour chiral expansions with good overall convergence:

$$A = A_{\rm LO} + A_{\rm NLO} + A\delta A\,, \quad \delta A \ll 1\,, \tag{8}$$

but the numerical balance between the leading-order $A_{\rm LO}$ and the next-to-leading-order $A_{\rm NLO}$ depends on the importance of vacuum fluctuations of $s\bar{s}$ pairs.

At the level of $O(p^4)$ $N_f = 3$ chiral perturbation theory, the size of the vacuum fluctuations is encoded in the low-energy constants (LECs) L_4 and L_6, whose values remain largely unknown. For a long time [13], they have been set to zero at an arbitrary hadronic scale (typically the η mass) assuming that the Zweig rule held in the scalar sector. More recent but indirect analyses based on dispersive methods [14, 24–26] suggest values of L_4 and L_6 which look quite modest but are sufficient to drive the $N_f = 3$ order parameters $\Sigma(3)$ and $F^2(3)$ down to half of their $N_f = 2$

[1] Let us stress that new data of high accuracy are expected from the NA48/2 Collaboration soon, which could affect these results significantly [8]. Recent lattice simulations with two-flavour dynamical quarks [9–12] may help to understand some aspects of these questions, even though the results are preliminary and rather delicate to interpret.

counterparts $\Sigma(2)$ and $F^2(2)$, leading to $A_{\rm LO} \simeq A_{\rm NLO}$ as recalled in Sect. 2.3. In addition, two-loop analyses [27–30] led to values of L_4 and L_6 off large-N_c expectations.

Unstable $N_f = 3$ chiral expansions ($A_{\rm LO} \sim A_{\rm NLO}$) demand a more careful treatment than in two-flavour χPT, in which such instabilities are seemingly absent. For instance, it would be wrong to believe that the chiral expansion of $1/A$ converges nicely.[2] This might induce the observed problems of convergence in recent two-loop computations [27–29]: the latter treat the fluctuations encoded in L_4 and L_6 as small and are not designed to cope with a large violation of the Zweig rule in the scalar sector, leading to instabilities of the chiral series.

Observables with a good convergence in the sense of (8) form a linear space, which we identify with connected QCD correlators of axial/vector currents and their derivatives, away from kinematic singularities. This choice promotes some "good" observables that can be extracted from such correlators, such as F_P^2 and $F_P^2 M_P^2$ ($P = \pi, K, \eta$): LO and NLO may compete, but there should be only a tiny contribution from NNLO and higher orders. On the contrary, the chiral expansion of M_P^2 (the ratio of the former quantities) may exhibit bad convergence. Similarly, the good observable associated with a form factor $F_{P\to Q}$ describing a transition from a pseudoscalar meson P to a meson Q will be $F_P F_Q F_{P\to Q}$, where the decay constants F_P and F_Q stem from wave-function renormalisation factors in the LSZ reduction formula.

2.2 One-loop bare expansion of QCD Green functions

In a previous work [16], we proposed a framework to deal with chiral expansions in the case of large fluctuations, by resumming the terms containing the Zweig rule violating LECs L_4 and L_6. This framework, which we will call resummed chiral perturbation theory (ReχPT), includes consistently the alternatives of large and small vacuum fluctuations. In this section, we explain how to expand a good observable at one loop in ReχPT. We addressed only energy-independent quantities in [16], where we explained in detail the similarities and differences of our approach with respect to generalized chiral perturbation theory [20–23].

We start from the one-loop generating functional for three-flavour χPT [13]:

$$Z = Z_{\rm t} + Z_{\rm u} + Z_{\rm A} + \dots\,, \tag{9}$$

where the ellipsis stands for NNLO contributions. The three terms of the one-loop generating functional are the following.

– $Z_{\rm t}$ is the sum of $O(p^2)$ and $O(p^4)$ tree graphs and of tadpole contributions:

$$Z_{\rm t} = \sum_P \int {\rm d}x \frac{F_0^2}{6} \left\{ 1 - \frac{3}{16\pi^2} \frac{\overset{\circ}{M}{}_P^2}{F_0^2} \log \frac{\overset{\circ}{M}{}_P^2}{\mu^2} \right\} \sigma^\Delta_{PP} + \sum_P \int {\rm d}x \frac{3F_0^2}{6} \left\{ 1 - \frac{3}{6\pi^2} \frac{\overset{\circ}{M}{}_P^2}{F_0^2} \log \frac{\overset{\circ}{M}{}_P^2}{\mu^2} \right\} \sigma^\chi_{PP} + \int {\rm d}x \mathcal{L}_4^{\rm r}\,, \tag{10}$$

where $F_0 \equiv F(3)$,

$$F_0 = F(3)\,, \quad B_0 = \frac{\Sigma(3)}{F(3)^2}\,, \quad r = \frac{m_s}{m}\,. \tag{11}$$

σ^Δ and σ^χ collect source terms for vector/axial currents and scalar/pseudoscalar densities, and $\mathcal{L}_4^{\rm r}$ is the $O(p^4)$ chiral Lagrangian with renormalised couplings $L_i^{\rm r}$ and $H_i^{\rm r}$. $\overset{\circ}{M}{}_P^2$ denotes the $O(p^2)$ contribution to the (squared) mass of the Goldstone boson P:

$$\begin{aligned} \overset{\circ}{M}{}_\pi^2 &= Y(3) M_\pi^2\,, \\ \overset{\circ}{M}{}_K^2 &= \frac{r+1}{2} Y(3) M_\pi^2\,, \\ \overset{\circ}{M}{}_\eta^2 &= \frac{2r+1}{3} Y(3) M_\pi^2\,. \end{aligned} \tag{12}$$

– $Z_{\rm u}$ collects unitarity corrections corresponding to one-loop graphs with two $O(p^2)$ vertices:

$$\begin{aligned} Z_{\rm u} = \sum_{P,Q} \int {\rm d}x\, {\rm d}y \Big[& \{ \{ \partial_{\mu\nu} - g_{\mu\nu} \Box \} M^{\rm r}_{PQ}(x-y) \\ & - g_{\mu\nu} L_{PQ}(x-y) \} \hat{\Gamma}^\mu_{PQ}(x) \hat{\Gamma}^\nu_{QP}(y) \\ & - \partial_\mu K_{PQ}(x-y) \hat{\Gamma}^\mu_{PQ}(x) \bar{\sigma}_{QP}(y) \\ & + \frac{1}{4} J^{\rm r}(x-y) \bar{\sigma}_{PQ}(x) \bar{\sigma}_{QP}(y) \Big]\,, \end{aligned} \tag{13}$$

where J, K, L, M are (renormalised) functions defined from the one-loop scalar integral with mesons P and Q propagating in the loop, and $\hat{\Gamma}^\mu$ and $\bar{\sigma} = \sigma^\Delta + \sigma^\chi$ collect source terms.

– $Z_{\rm A}$ is the Wess–Zumino functional collecting anomalous contributions.

The one-loop functional (9) has been derived using the propagators and couplings of the $O(p^2)$ chiral Lagrangian, and therefore it is expressed only in terms of chiral couplings: F_0 and B_0, L_i … [13]. In particular, the Goldstone degrees of freedom have masses truncated at $O(p^2)$, denoted $\overset{\circ}{M}{}_P^2$. Large fluctuations should induce significant differences between this quantity and the physical mass M_P^2. Therefore, we want to replace $\overset{\circ}{M}{}_P^2$ by M_P^2 only when justified by physics arguments, since this replacement may have an important impact when comparing chiral expansions with the experimental data.

– The anomalous contribution $Z_{\rm A}$ corresponds to local couplings for vector and axial currents and is not affected by our discussion.

– For the unitarity corrections $Z_{\rm u}$, were we to consider higher and higher orders of the chiral expansion, we should obtain that the masses occurring in the functions $J^{\rm r}$, K, L and $M^{\rm r}$ are physical masses, in order

[2] This would be equivalent to claiming that $1/(1+x) \simeq 1-x$ is a reasonable approximation for $x = O(1)$.

to get the low-mass two-particle cuts at the physical positions. Therefore, we write those functions with the physical masses of the Goldstone bosons. On the contrary, we keep the multiplying factors Γ^μ and $\bar\sigma$ expressed in terms of the parameters of the effective Lagrangian (m_q, B_0, ...).

– The tadpole contributions present in $Z_{\rm t}$ are derived using the $O(p^2)$ contribution to the Goldstone boson masses $\overset{\circ}{M}{}^2_P$. In [16], we have proposed the replacement

$$\frac{\overset{\circ}{M}{}^2_P}{32\pi^2}\log\frac{\overset{\circ}{M}{}^2_P}{\mu^2} \quad\to\quad \frac{\overset{\circ}{M}{}^2_P}{32\pi^2}\log\frac{M^2_P}{\mu^2}\,. \tag{14}$$

We could have kept $\overset{\circ}{M}{}^2_P$ everywhere in $Z_{\rm t}$, and in particular inside the logarithm. However, the resulting expressions are easier to deal with, and the change has only a tiny numerical impact: either M_P is close to its $O(p^2)$ term and the change is trivially justified, or $\overset{\circ}{M}{}^2_P$ is much smaller than M^2_P and the whole tadpole contribution is very small.

– Physical S-matrix elements are obtained from the Green functions derived with the generating functional by applying the LSZ reduction formula. The external legs corresponding to incoming and outgoing particles must be put on the mass shell. In the process, the products of the external momenta are translated into the well-known Mandelstam variables. These kinematical relations are valid for physical masses, and we will use the latter (and not the $O(p^2)$ truncated masses $\overset{\circ}{M}{}^2_P$) whenever we reexpress products of external momenta. This prescription is consistent with the use of physical masses in the one-loop scalar integral present in the unitarity term $Z_{\rm u}$.

Following the renormalisation procedure in [13], one can easily check that (14) does not change the renormalisation-scale dependence of LECs at one loop. Actually, the whole one-loop generating functional Z becomes exactly renormalisation-scale independent: when we follow the prescription given above, all the scale-dependent logarithms present in $Z_{\rm t}$ (explictly shown in (10)) and $Z_{\rm u}$ (hidden in the one-loop functions $M^{\rm r}$ and $J^{\rm r}$ in (13)) are multiplied by terms of the same form, m_qB_0, and thus cancel exactly. In the more usual treatment of the tadpoles [13], m_qB_0 terms are replaced by physical Goldstone masses in the one-loop generating functional (see Sect. 8 in [13]). In this case, the cancellation of the logarithms takes place only up to $O(p^4)$, and some higher-order logarithmic pieces of $Z_{\rm t}$ have no counterpart in $Z_{\rm u}$.

We call the chiral expansion treated according to our prescription a "bare expansion", because we prefer keeping the original couplings of the chiral Lagrangian to trading them for physical masses and decay constants. We sum up our method to obtain bare expansions of Green functions in resummed χPT:

1. Consider a subset of observables suitable for a chiral expansion, such as the linear space of connected QCD correlators of axial/vector currents and their derivatives away from kinematic singularities.
2. Extract the bare expansion of the observables using the one-loop generating functional (9): in $Z_{\rm t}$, replace the tadpole contributions by (14), and in $Z_{\rm u}$, use the physical masses for the functions J, K, L, M defined from the one-loop scalar integral.
3. Use physical masses to reexpress scalar products of external momenta in terms of the Mandelstam variables.
4. Keep track of the higher-order contributions by introducing remainders, i.e. NNLO quantities that have an unknown value but are assumed to be small enough for the chiral series to converge.
5. Exploit algebraically the resulting relations, and never trade the couplings of the chiral Lagrangian for observables, while neglecting higher-order terms.

The main differences from the usual treatment of three-flavour chiral series consist in the choice of a particular subset of observables, the distinction between physical meson masses and their $O(p^2)$ truncated forms, and the algebraic use of the chiral expansions, while keeping track of higher-order terms explicitly.

2.3 Masses and decay constants of Goldstone bosons

The first example consists in pseudoscalar decay constants and masses. The usual χPT expressions (Sect. 10 in [13]) become the following bare expansions in ReχPT (similar expressions for η can be found in [16, 34]):

$$\begin{aligned} F_\pi^2 &= F_\pi^2 Z(3) + 8(r+2)Y(3)M_\pi^2\Delta L_4 \\ &\quad + 8Y(3)M_\pi^2\Delta L_5 + F_\pi^2 e_\pi\,, \end{aligned} \tag{15}$$

$$\begin{aligned} F_K^2 &= F_\pi^2 Z(3) + 8(r+2)Y(3)M_\pi^2\Delta L_4 \\ &\quad + 4(r+1)Y(3)M_\pi^2\Delta L_5 + F_K^2 e_K\,, \end{aligned} \tag{16}$$

$$\begin{aligned} F_\pi^2 M_\pi^2 &= F_\pi^2 M_\pi^2 X(3) + 16(r+2)Y^2(3)M_\pi^4\Delta L_6 \\ &\quad + 16Y^2(3)M_\pi^4\Delta L_8 + F_\pi^2 M_\pi^2 d_\pi\,, \end{aligned} \tag{17}$$

$$\begin{aligned} F_K^2 M_K^2 &= \frac{r+1}{2}F_\pi^2 M_\pi^2 X(3) \\ &\quad + 8(r+2)(r+1)Y^2(3)M_\pi^4\Delta L_6 \\ &\quad + 4(r+1)^2Y^2(3)M_\pi^4\Delta L_8 + F_K^2 M_K^2 d_K\,. \end{aligned} \tag{18}$$

We take as free parameters the $N_f = 3$ quark condensate and the pseudoscalar decay constant expressed in physical units[3], as well as their ratio and the quark mass ratio:

$$\begin{aligned} X(3) &= \frac{2m\Sigma(3)}{F_\pi^2 M_\pi^2}\,, \quad Z(3) = \frac{F^2(3)}{F_\pi^2}\,, \\ Y(3) &= \frac{X(3)}{Z(3)} = \frac{2mB_0}{M_\pi^2}\,. \end{aligned} \tag{19}$$

[3] In this paper, we work in the isospin symmetry limit, where $m_u = m_d = m$ and the electromagnetic interaction is ignored. We take the following values for the masses and decay constants: $F_\pi = 92.4\,\text{MeV}$, $F_K/F_\pi = 1.22$, $M_\pi = 139.6\,\text{MeV}$, $M_K = 495.7\,\text{MeV}$, $M_\eta = 547\,\text{MeV}$.

We have introduced the NNLO remainders d_π, e_π, d_K and e_K, and the combinations of LECs and chiral logarithms:

$$\Delta L_4 = L_4^{\rm r}(\mu) - \frac{1}{256\pi^2}\log\frac{M_K^2}{\mu^2} + \frac{1}{128\pi^2}\frac{r}{(r-1)(r+2)} \times\left\{\log\frac{M_K^2}{M_\pi^2}+\left(1+\frac{1}{2r}\right)\log\frac{M_\eta^2}{M_\pi^2}\right\}, \tag{20}$$

$$\Delta L_5 = L_5^{\rm r}(\mu) - \frac{1}{256\pi^2}\left[\log\frac{M_K^2}{\mu^2}+2\log\frac{M_\eta^2}{\mu^2}\right] - \frac{1}{256\pi^2(r-1)}\left(3\log\frac{M_\eta^2}{M_K^2}+5\log\frac{M_K^2}{M_\pi^2}\right). \tag{21}$$

$$\Delta L_6 = L_6^{\rm r}(\mu) - \frac{1}{512\pi^2}\left(\log\frac{M_K^2}{\mu^2}+\frac{2}{9}\log\frac{M_\eta^2}{\mu^2}\right) + \frac{1}{512\pi^2}\frac{r}{(r+2)(r-1)}\left(3\log\frac{M_K^2}{M_\pi^2}+\log\frac{M_\eta^2}{M_K^2}\right). \tag{22}$$

$$\Delta L_8 = L_8^{\rm r}(\mu) - \frac{1}{512\pi^2}\left[\log\frac{M_K^2}{\mu^2}+\frac{2}{3}\log\frac{M_\eta^2}{\mu^2}\right] - \frac{1}{512\pi^2(r-1)}\left(3\log\frac{M_K^2}{M_\pi^2}+\log\frac{M_\eta^2}{M_K^2}\right). \tag{23}$$

The values of the logarithms are only mildly dependent on r; for $r=25$,

$$\Delta L_4 = L_4^{\rm r}(M_\rho)+0.51\times10^{-3},$$
$$\Delta L_5 = L_5^{\rm r}(M_\rho)+0.67\times10^{-3}, \tag{24}$$
$$\Delta L_6 = L_6^{\rm r}(M_\rho)+0.26\times10^{-3},$$
$$\Delta L_8 = L_8^{\rm r}(M_\rho)+0.20\times10^{-3}. \tag{25}$$

Since F_π, F_K, M_π and M_K are accurately known, we can use these expressions to eliminate some of the $O(p^4)$ LECs in the chiral expansion of the other observables. This is rather different from the usual χPT trading, since we explicitly keep higher-order terms that would have been neglected in the usual (perturbative) treatment of chiral series.

From the masses and decay constants (15)–(18), we get the equivalent set of equations providing some $O(p^4)$ LECs in terms of physical masses and decay constants, $r, X(3), Y(3)$ and NNLO remainders:

$$Y^2(3)\Delta L_6 = \frac{1}{16(r+2)}\frac{F_\pi^2}{M_\pi^2}[1-\epsilon(r)-X(3)-d], \tag{26}$$

$$Y^2(3)\Delta L_8 = \frac{1}{16}\frac{F_\pi^2}{M_\pi^2}[\epsilon(r)+d'], \tag{27}$$

$$Y(3)\Delta L_4 = \frac{1}{8(r+2)}\frac{F_\pi^2}{M_\pi^2}[1-\eta(r)-Z(3)-e], \tag{28}$$

$$Y(3)\Delta L_5 = \frac{1}{8}\frac{F_\pi^2}{M_\pi^2}[\eta(r)+e'], \tag{29}$$

with

$$\epsilon(r) = 2\frac{r_2-r}{r^2-1}, \quad \eta(r) = \frac{2}{r-1}\left(\frac{F_K^2}{F_\pi^2}-1\right), \tag{30}$$

and the following linear combinations of NNLO remainders arise:

$$d = \frac{r+1}{r-1}d_\pi - \left(\epsilon(r)+\frac{2}{r-1}\right)d_K, \quad d' = d-d_\pi, \tag{31}$$

$$e = \frac{r+1}{r-1}e_\pi - \left(\eta(r)+\frac{2}{r-1}\right)e_K, \quad e' = e-e_\pi. \tag{32}$$

The above identities are algebraically exact, but they are useful only as long as the NNLO remainders are small. In [16, 34], the size of the NNLO remainders was taken to be

$$d, e = O(m_s^2)\sim 10\%, \quad d', e' = O(mm_s)\sim 3\%, \tag{33}$$

with the rule of thumb that NNLO corrections of size $O(m_s^2)$ should not exceed $(30\%)^2\simeq 10\%$ of the contribution to the observable while $O(m_s m)$ terms would be less than $30\%\cdot 10\%\simeq 3\%$. We will propose in the next section a different but compatible way of dealing with this issue.

In (26)–(29), the presence of powers of $Y(3)$, i.e., B_0, follows from the normalisation of the scalar and pseudoscalar sources in [13]: these powers arise only for $O(p^4)$ LECs related to explicit chiral symmetry breaking (two powers for L_6, L_7, L_8, one for L_4 and L_5) and are absent for LECs associated with purely derivative terms.

2.4 From bare expansions to ReχPT expansions

As shown in detail in [15], plugging (26)–(29) into the bare expansions for other observables corresponds to resumming the vacuum fluctuations encoded in L_4 and L_6. As an illustration, we recall that we can exploit (26)–(29) to relate $Y(3)$ to the chiral couplings L_4 and L_6:

$$Y(3) = \frac{2[1-\epsilon(r)-d]}{[1-\eta(r)-e]+\sqrt{[1-\eta(r)-e]^2+k[2\Delta L_6-\Delta L_4]}}, \tag{34}$$

$$k = 32(r+2)\frac{M_\pi^2}{F_\pi^2}[1-\epsilon(r)-d]. \tag{35}$$

If vacuum fluctuations are small, i.e. if ΔL_6 and ΔL_4 are almost vanishing, one can treat $k\times[2\Delta L_6-\Delta L_4]$ in the denominator as a small perturbation and linearise the equation as $Y(3)=1+O(p^2)$. This corresponds to the usual (iterative and perturbative) treatment of the chiral series. However, the factor k is very large ($k\simeq 1900$ for $r=25$) and values of ΔL_6 and ΔL_4 of a few 10^{-3} suffice to yield an important deviation of $Y(3)$ from 1, while the linear approximation becomes inaccurate. Similar relations exist between $X(3)$ and ΔL_6, and between $Z(3)$ and ΔL_4 [15].

Using (26)–(29), we obtain the one-loop expansions of good observables in ReχPT, by using (26)–(29) and reexpressing $F(3)$, mB_0, $Y(3)L_4$, $Y(3)L_5$, $Y(3)^2L_6$, $Y(3)^2L_8$

(and $Y(3)^2 L_7$ through the η identities) in terms of the three parameters of interest $X(3)$, $Z(3)$, r and NNLO remainders. In the case of $\pi\pi$ and πK scatterings, only three $O(p^4)$ LECs (L_1, L_2 and L_3) will remain. The square root induced by equations like (34) is a non-perturbative feature of our framework. It amounts to resumming (potentially) large contributions of vacuum fluctuations, encoded in the Zweig rule violating LECs L_4 and L_6. This feature, in contrast with the usual treatment of chiral series, has led us to call our framework resummed chiral perturbation theory or ReχPT.

There is a price to pay for this extension of the chiral framework in the case of large fluctuations of $s\bar{s}$ pairs and the resulting competition between LO and NLO in the chiral counting: some usual $O(p^4)$ relations cannot be exploited anymore, because of our ignorance about their convergence. For instance, the quark mass ratio $r = m_s/m$ ($m = m_u = m_d$) cannot be fixed from M_K^2/M_π^2 since we do not control the convergence of its three-flavour chiral expansion. r becomes a free parameter that can vary in the range

$$r_1 = 2\frac{F_K M_K}{F_\pi M_\pi} - 1 \sim 8 \leq r \leq r_2 = 2\frac{F_K^2 M_K^2}{F_\pi^2 M_\pi^2} - 1 \sim 36\,. \tag{36}$$

Similarly, one cannot determine LECs or combinations of LECs through ratios of observables. For instance, one should not use F_K/F_π to determine L_5 at $O(p^4)$, because we do not know if the chiral expansion of F_K/F_π converges at all. Finally, the agreement of the pseudoscalar spectrum with the Gell-Mann–Okubo formula requires a fine tuning of L_7 (however, this fine tuning is also needed in the case of a dominant $N_f = 3$ quark condensate and small vacuum fluctuations [16]).

3 $\pi\pi$ and πK scattering amplitudes

In this section, we are applying the ReχPT framework to two examples of Goldstone boson scatterings: $\pi\pi$ scattering, which probes the structure of QCD vacuum in the $N_f = 2$ chiral limit, and πK scattering, which is linked with the $N_f = 3$ chiral limit.

3.1 One-loop expression in ReχPT

In the isospin symmetry limit, the low-energy $\pi\pi$ scattering is described by a single Lorentz-invariant amplitude:

$$\begin{aligned} &A(\pi^a(p_1) + \pi^b(p_2) \to \pi^c(p_3) + \pi^d(p_4)) \\ &= \delta^{ab}\delta^{cd} A(s,t,u) + \delta^{ac}\delta^{bd} A(t,u,s) + \delta^{ad}\delta^{bc} A(u,t,s)\,, \end{aligned} \tag{37}$$

where the usual Mandelstam variables are

$$s = (p_1+p_2)^2\,, \quad t = (p_1-p_3)^2\,, \quad u = (p_1-p_4)^2\,, \tag{38}$$

and A is symmetric under $t \leftrightarrow u$ exchange. In a similar way, we consider low-energy πK scattering, which can be decomposed into two amplitudes according to isospin in the s-channel $I = 3/2$ and $I = 1/2$:

$$A(\pi^a(p_1) + K^i(p_2) \to \pi^b(p_3) + K^j(p_4)) = F_{\pi K}^I(s,t,u)\,, \tag{39}$$

from which one can define two amplitudes, respectively even and odd under $s \leftrightarrow u$ exchange:

$$B(s,t,u) = \frac{2}{3}F_{\pi K}^{3/2}(s,t,u) + \frac{1}{3}F_{\pi K}^{1/2}(s,t,u)\,, \tag{40}$$

$$C(s,t,u) = -\frac{1}{3}F_{\pi K}^{3/2}(s,t,u) + \frac{1}{3}F_{\pi K}^{1/2}(s,t,u)\,. \tag{41}$$

In addition, crossing symmetry provides a relation between the two amplitudes:

$$F_{\pi K}^{1/2}(s,t,u) = \frac{3}{2}F_{\pi K}^{3/2}(u,t,s) - \frac{1}{2}F_{\pi K}^{3/2}(s,t,u)\,. \tag{42}$$

We can apply the prescriptions described in Sect. 2.2 to determine the one-loop ReχPT expansions of A, B and C. The relevant good observables, which can be derived from Green functions of vector/axial currents, are $F_\pi^4 A$, $F_\pi F_K F$ and $F_\pi F_K G$.

1. We determine the one-loop bare expansions of these quantities. This can be done using the generating functional of $N_f = 3$ χPT [13], with the essential difference that we keep the distinction between $O(p^2)$ truncated masses and physical masses of the Goldstone bosons. This was performed in the case of πK scattering in [35]. A similar work can be done in the case of $\pi\pi$ scattering. The corresponding (rather lengthy) expressions are summarised in Appendix A.
2. We use (20)–(23) to reexpress the $O(p^4)$ LECs L_4, L_5, L_6 and L_8 in terms of r, $X(3)$ and $Z(3)$, and the NNLO remainders related to π and K masses and decay constants. We denote with the superscript LO + NLO the resulting expressions, which include the LO and NLO expansions of the relevant good observables and resum the vacuum fluctuations encoded in L_4 and L_6.
3. To obtain the ReχPT expansions of the $\pi\pi$ and πK scattering amplitudes, we add to the resulting expressions a polynomial modeling higher-order contributions:

$$\begin{aligned} F_\pi^4 A^{\mathrm{Re}\chi\mathrm{PT}} &= F_\pi^4 A^{\mathrm{LO+NLO}} \\ &\quad + F_\pi^2(s_\mathrm{A} - M_\pi^2)a_1 + F_\pi^2(s - s_\mathrm{A})a_2 \\ &\quad + (s-s_\mathrm{A})^2 a_3 \\ &\quad + [(t-t_\mathrm{A})^2 + (u-u_\mathrm{A})^2]a_4\,, \end{aligned} \tag{43}$$

$$\begin{aligned} F_\pi^2 F_K^2 B^{\mathrm{Re}\chi\mathrm{PT}} &= F_\pi^2 F_K^2 B^{\mathrm{LO+NLO}} \\ &\quad + F_\pi F_K t_B b_1 + F_\pi F_K (t - t_B) b_2 \\ &\quad + (t-t_B)^2 b_3 \\ &\quad + [(s-s_B)^2 + (u-u_B)^2]b_4\,, \end{aligned} \tag{44}$$

$$\begin{aligned} F_\pi^2 F_K^2 C^{\mathrm{Re}\chi\mathrm{PT}} &= F_\pi^2 F_K^2 C^{\mathrm{LO+NLO}} \\ &\quad + F_\pi F_K (s-u)c_1 + (t-t_B)(s-u)c_2\,, \end{aligned} \tag{45}$$

where $(s_\mathrm{A}, t_\mathrm{A}, u_\mathrm{A})$, (s_B, t_B, u_B), (s_C, t_C, u_C) denote the points around which we perform the expansion of the NNLO polynomial. The first remainder is multiplied by

a constant estimating roughly the value of the amplitude at the expansion point (obtained from the LO chiral expression). The other remainders are multiplied by polynomials in the Mandelstam variables that vanish at the expansion point and respect the crossing properties of the amplitude.

For our purposes, we take

$$(s_A, t_A, u_A) = (4/3M_\pi^2, 4/3M_\pi^2, 4/3M_\pi^2)\,, \tag{46}$$

$$\begin{aligned}(s_B, t_B, u_B) &= (s_C, t_C, u_C)\\ &= (M_K^2 + 1/3M_\pi^2, 4/3M_\pi^2, M_K^2 + 1/3M_\pi^2)\,.\end{aligned} \tag{47}$$

The remainders a_i, b_i, c_i include only NNLO terms or higher: we expect therefore these contributions to be suppressed by $1/\Lambda_H^4$, where Λ_H is a typical hadronic scale [36, 37]. On the other hand, the numerator may depend on the remainder considered, but the contribution to the polynomial must be of order $O(p^6)$ in the usual chiral counting. This means that the remainders have a typical size of order

$$a_1, a_2, b_1, b_2, c_1 \sim \frac{M_K^4}{\Lambda_H^4}\,, \quad a_3, a_4, b_3, b_4, c_2 \sim \frac{F_\pi^2 M_K^2}{\Lambda_H^4}\,. \tag{48}$$

Remainders associated with higher-order polynomials would be of order F_π^4/Λ_H^4, much suppressed compared to the terms considered here, and thus neglected in the following analysis.

In the case of $\pi\pi$ scattering, we can exploit the behaviour of the amplitude in the $N_f = 2$ chiral limit in order to constrain the size of the NNLO remainders further. Indeed, from $N_f = 2$ chiral perturbation theory, we know that

$$F_\pi^4 A(s,t,u) - F_\pi^2(s - M_\pi^2) = O(\epsilon^4) \text{ with } \epsilon^2 \sim p^2 \sim m\,. \tag{49}$$

ϵ counts only powers of $m = m_u = m_d$ but not those of m_s. If we compare this relation with $F_\pi^4 A$ expressed in $N_f = 3$ ReχPT in (43) and (A.3), we see that the relation (49) implies a constraint on the NNLO remainders: $a_1 - e_\pi - (d_\pi - e_\pi)/3/(s_A/M_\pi^2 - 1)$ and $a_2 - e_\pi$ must be proportional to m. Therefore, we can expect the remainders to exhibit the typical sizes

$$a_1 - e - \frac{d-e}{3(s_A/M_\pi^2 - 1)}, \quad a_2 - e \sim \frac{M_\pi^2 M_K^2}{\Lambda_H^4}\,, \tag{50}$$

$$b_1, b_2, c_1 \sim \frac{M_K^4}{\Lambda_H^4}\,, \quad a_3, a_4, b_3, b_4, c_2 \sim \frac{F_\pi^2 M_K^2}{\Lambda_H^4}\,.$$

According to this discussion, we take the following ranges for the direct remainders:

$$a_1 - e - \frac{F_\pi^2 M_\pi^2}{3(s_A - M_\pi^2)}(d-e)\,, \tag{51}$$

$$a_2 - e \in \left[-\frac{2M_\pi^2 M_K^2}{\Lambda_H^4}, \frac{2M_\pi^2 M_K^2}{\Lambda_H^4}\right]\,,$$

$$b_1, b_2, c_1 \in \left[-\frac{M_K^4}{\Lambda_H^4}, \frac{M_K^4}{\Lambda_H^4}\right]\,,$$

$$a_3, a_4, b_3, b_4, c_2 \in \left[-\frac{F_\pi^2 M_K^2}{\Lambda_H^4}, \frac{F_\pi^2 M_K^2}{\Lambda_H^4}\right]\,,$$

with $\Lambda_H = 0.85$ GeV. This choice for the numerical value of Λ_H provides good agreement of our estimates with those used in [1, 5, 16] for energy-independent quantities. In the latter references, the NNLO remainders were taken of order $O(m_s^2) = (30\%)^2 = 10\%$ of the leading-order value, unless they were suppressed by one power of m and thus of order $O(mm_s) = 30\% \times 10\% = 3\%$. According to this work, the same remainders must remain respectively of order $M_K^4/\Lambda_H^4 = 12\%$ and $2M_\pi^2 M_K^2/\Lambda_H^4 = 2\%$. In addition, one can check that the definition and size of the remainders given in this section can be applied to the two-point correlators related to F_P^2 and $F_\pi^2 M_\pi^2$ with an expansion around the point of vanishing transfer momentum, leading to remainders identical to those defined in Sect. 2.3.

3.2 Roy and Roy–Steiner equations

The above theoretical expressions for low-energy $\pi\pi$ and πK scattering must be compared to experimental information in order to extract the parameters of three-flavour chiral symmetry breaking. Fortunately, dispersion relations provide an appropriate framework to analyse the experimental data and extract the low-energy behaviour of the amplitude, through the Roy and Roy–Steiner equations.

In [4], the Roy equations were derived and solved with experimental input on high-energy $\pi\pi$ scattering. The solutions were parametrised in terms of the two scattering lengths a_0^0 and a_0^2. In [4, 5], these solutions, and some of their extensions, were exploited together with recent data on $\pi\pi$ scattering in order to determine the low-energy structure of the amplitude with the best accuracy. Reference [6] proposed to combine $K_{\ell 4}$ data on $\delta_0^0 - \delta_1^1$ supplemented with a theoretical constraint from the scalar radius of the pion. This constraint was assessed critically in [5], where it was proposed to avoid any reference to the scalar radius of the pion and to rely only on the experimental data, namely $K_{\ell 4}$ data supplemented with $I = 2$ data. We follow the latter approach and take the results of the so-called "Global" fit, (12) in [5], for the $\pi\pi$ scattering data.

In [14], the Roy–Steiner equations were investigated to study the πK scattering amplitude. In spite of recent progress in $\tau \to K\pi\nu_\tau$ and $D \to K\pi e\nu_e$ decays, low-energy data on πK phase shifts are still lacking. However, the dispersive analysis of the data in the intermediate region turned out to provide rather tight constrains on the low-energy πK amplitude. We use the results of [14] for πK scattering.

It is a straightforward, if tedious, exercise, to exploit the dispersive representations of the amplitudes A, B and C found in Sect. 3 of [4] and in Sect. 2 of [14], and to compute them in subthreshold regions, where none of the dispersion integrals exhibit singularities. We checked in particular that our representation of the low-energy πK amplitude was in good numerical agreement with the subthreshold expansion presented in Sect. 6.3 in [14].

We define the subthreshold region of interest for $\pi\pi$ scattering as a triangle in the Mandelstam plane delimited by points with (s,t,u):

$$(2M_\pi^2, M_\pi^2, M_\pi^2)\,, \quad (M_\pi^2/2, 3/2M_\pi^2, 3/2M_\pi^2)\,, \\ (M_\pi^2/2, 3M_\pi^2, M_\pi^2/2)\,, \tag{52}$$

taking into account the symmetry of the amplitude under t–u exchange. Similarly, we define for πK scattering a triangle in the Mandelstam plane with

$$(M_K^2, 2M_\pi^2, M_K^2)\,, \quad (M_K^2, 0, M_K^2+2M_\pi^2)\,, \\ (M_K^2+M_\pi^2, 0, M_K^2+M_\pi^2)\,, \tag{53}$$

exploiting the symmetry or antisymmetry under s–u exchange. In each triangle, we defined 15 points regularly spaced where we compute the scattering amplitudes. Some aspects of the computation, and of the correlations among the points, are covered in Appendix B.

4 Matching in a frequentist approach

We must match the chiral expansions of the scattering amplitudes with the experimental values described in the previous section. We perform this matching in a frequentist approach inspired by the Rfit method [17].

4.1 Likelihood

We collect in a vector V our $3n$ observables:

$$V^{\mathrm{T}} = [A(s_1,t_1)\dots A(s_n,t_n), B(s_1',t_1')\dots B(s_n',t_n'), \\ C(s_1'',t_1'')\dots C(s_n'',t_n'')]\,. \tag{54}$$

Since we use the masses and decay constant identities for pions and kaons to reexpress the $O(p^4)$ LECs in terms of F_P^2 and $F_P^2M_P^2$ through (26)-(29), our set of theoretical parameters is

$$\text{Parameters}: \; r, X(3), Z(3), L_1^{\mathrm{r}}, L_2^{\mathrm{r}}, L_3\,, \tag{55}$$

$$\text{Direct remainders}: \; a_1,a_2,a_3,a_4,b_1,b_2,b_3,b_4,c_1,c_2\,, \tag{56}$$

$$\text{Indirect remainders}: \; d,d',e,e',d_X,d_Z\,. \tag{57}$$

We have separated the direct remainders, attached to the bare expansions of the observables, and the indirect remainders, arising through the reexpression of $O(p^4)$ LECs thanks to mass and decay constant equalities. The latter include also the remainders d_X and d_Z, whose expressions will be given in Sect. 4.2 and which are required to express the paramagnetic constraints on X and Z, (5).

We construct the experimental likelihood $\mathcal{L}_{\mathrm{exp}}$, i.e. the probability of observing the data for a given choice of the theoretical parameters T_n:

$$\mathcal{L}_{\mathrm{exp}}(T_n) = P(\mathrm{data}|T_n) \\ \propto \exp\left(-\frac{1}{2}(V_{\mathrm{th}}-V_{\mathrm{exp}})^{\mathrm{T}}C^{-1}(V_{\mathrm{th}}-V_{\mathrm{exp}})\right)/\sqrt{\det C}\,. \tag{58}$$

To avoid a proliferation of (purely numerical) normalisation factors of no significance for our discussion, we use the sign $\propto$ meaning "proportional to". C is the covariance matrix between the experimental values V_{exp} computed through (B.2), whereas V_{th} denotes the theoretical values computed with the particular choice of T_n. Since we expect strong correlations among the parameters, the covariance matrix must be treated with some care, as described in Appendix C.

The theoretical likelihood $\mathcal{L}_{\mathrm{th}}(T_n)$ describes our current knowledge on the parameters of the theory. In agreement with the Rfit prescription [17], we consider that $\mathcal{L}_{\mathrm{th}}(T_n)=1$ if each theoretical parameter lies within its allowed range described in the next section; otherwise the likelihood vanishes.

4.2 Constraints on the theoretical parameters

To build the theoretical likelihood, we impose a list of constraints on the theoretical parameters. Some constraints are fairly simple.

- We take the following range for the ratio of quark masses r:

$$r_1 \le r \le r_2\,, \\ r_1 = 2\frac{F_KM_K}{F_\pi M_\pi}-1\,, \quad r_2 = 2\left(\frac{F_KM_K}{F_\pi M_\pi}\right)^2-1\,. \tag{59}$$

- Vacuum stability yields constraints on the $N_f=3$ chiral order parameters:

$$X(3)\ge 0\,, \quad Z(3)\ge 0\,. \tag{60}$$

- We allow the three $O(p^4)$ LECs $L_1^{\mathrm{r}}(M_\rho), L_2^{\mathrm{r}}(M_\rho), L_3$ to be in the range $[-F_\pi^2/\Lambda_{\mathrm{H}}^2, F_\pi^2/\Lambda_{\mathrm{H}}^2]$, i.e. lower than 12×10^{-3} in absolute value.
- The direct remainders are constrained to remain in the range given in (51).
- The indirect remainders must lie in the ranges discussed in Sect. 3.1:

$$d',e',d_X,e_X \in \left[-\frac{2M_\pi^2M_K^2}{\Lambda_{\mathrm{H}}^4}, \frac{2M_\pi^2M_K^2}{\Lambda_{\mathrm{H}}^4}\right]\,, \\ d,e \in \left[-\frac{M_K^4}{\Lambda_{\mathrm{H}}^4}, \frac{M_K^4}{\Lambda_{\mathrm{H}}^4}\right]\,, \tag{61}$$

  i.e. 3% for the first and 12% for the latter.

A second set of constraints translates into bounds on combinations of the remainders.

- Vacuum stability for $N_f=2$ chiral order parameters yields

$$X(2)\ge 0 \leftrightarrow d \le d_{\max} \equiv 1-\epsilon(r)-Y(3)^2\times L_X\,, \tag{62}$$

$$Z(2)\ge 0 \leftrightarrow e \le e_{\max} \equiv 1-\eta(r)-Y(3)\times L_Z\,, \tag{63}$$

  where L_X and L_Z are small combinations of chiral logarithms denoted f_1 and g_1 in [15,16]. These chiral logarithms involve M_K and M_η in the $N_f=2$ chiral limit,

which can be computed through the iterative method presented in [15].

– The paramagnetic inequalities (5) lead to

$$X(3) \leq X(2) \leftrightarrow d_X \geq d_{X,\min} \equiv 1 - \frac{d_{\max} - d}{X(3)(1-d)}\,, \tag{64}$$

$$Z(3) \leq Z(2) \leftrightarrow e_Z \geq e_{Z,\min} \equiv 1 - \frac{e_{\max} - e}{Z(3)(1-e)}\,. \tag{65}$$

– The ratio of order parameters $Y(3) = X(3)/Z(3) = 2mB_0/M_\pi^2$ is bound [15]:

$$Y(3) \leq Y^{\max} = 2\frac{1-\epsilon(r)-d}{1-\eta(r)-e}\,. \tag{66}$$

4.3 Computation of the confidence level

Contrary to [16], which adopted a Bayesian approach to deal with $\pi\pi$ scattering, we follow the (frequentist) Rfit procedure advocated in [17] and used for the analysis of the CKM matrix in [38]. From the theoretical and experimental likelihoods we define the function of the theoretical parameters

$$\chi^2(T_n) = -2\log\mathcal{L}(T_n) = -2\log[\mathcal{L}_{\rm th}(T_n)\mathcal{L}_{\rm exp}(T_n)]\,. \tag{67}$$

We start by computing the absolute minimum of χ^2, letting all theoretical parameters vary freely; we denote this value by $\chi^2_{\rm min;all}$. Then we focus on one particular theoretical parameter T_i. We assume that it reaches a particular value t_i and compute the minimum:

$$\chi^2_{\rm min;not\ }{}_i(t_i) = \min\{\chi^2(T_n); T_i = t_i\}\,. \tag{68}$$

Then we compute the corresponding confidence level:

$$\mathcal{P}(t_i) = {\rm Prob}[\chi^2_{\rm min;not\ }{}_i(t_i) - \chi^2_{\rm min;all}, 1]\,, \tag{69}$$

where ${\rm Prob}(c^2, N_{\rm dof})$ is the routine from the CERN library providing the probability that a random variable having a χ^2-distribution with $N_{\rm dof}$ degrees of freedom assumes a value that is larger than c^2. Admittedly, we are simplifying the statistical problem at hand, since we assume that the function $\chi^2(t_i)$ has indeed a χ^2-distribution. This should be a correct assumption if the experimental component is free from non-Gaussian contributions and inconsistent measurements [17].

This method provides an upper bound on the marginal confidence level (CL) of $T_i = t_i$ for the optimal set of theoretical parameters: the CL value is the probability that a new series of measurements will agree with the most favourable set of theoretical parameters (at $T_i = t_i$) in a worse way than the experimental results actually used in the analysis [18, 19]. The value of t_i for which $\mathcal{P}(t_i)$ is maximal provides an estimator of T_i: in the ideal case of very accurate data in excellent agreement with theoretical expectations, $\mathcal{P}(t_i)$ should exhibit a sharp peak indicating the "true" value of T_i.

We have implemented this procedure in a program. Before turning to Goldstone boson scattering, we checked the validity of our programs using "fake" observables. We designed observables with very simple chiral representations (linear or quadratic dependence on $r, X(3), Z(3)$) and we simulated a set of data with a certain choice of $r, X(3), Z(3)$, adding some random noise. We plugged these "data" into our program and computed the confidence level for each theoretical parameter, r, $X(3)$ and $Z(3)$. When the chiral representation of the observables depended on this parameter, we obtained a function $\mathcal{P}(t_i)$ showing a peak in agreement with the value used to simulate the data (i.e., we recovered the information contained in the data). When the chiral series for the observables had no dependence on the parameter, the function $\mathcal{P}(t_i)$ was flat (i.e., we did not extract information absent from the data).

5 Results

In this section, we discuss the results obtained by matching the one-loop ReχPT expansions and the dispersive results on $\pi\pi$ and πK scattering, relying on the frequentist approach described in the previous section.

5.1 CL for order parameters and related quantities

We have plotted the confidence level of the order parameters $X(3), Y(3)$ and $Z(3)$, as well as the quark mass ratio r. In each case, the dashed line indicates the results obtained from $\pi\pi$ scattering, the dotted line from πK scattering, while the solid line stems from the combination of both pieces of information.

If we include $\pi\pi$ scattering only, we see that small values of r, below 13, are disfavoured (this is also the case for large values of r above 25, but not at a significant level): $r \geq 12$ at 68% CL. The CL for $X(3)$ is flat up to 0.85, where it suddenly drops, as well as that for $Z(3)$ up to 0.95. $Y(3)$, which is related to B_0 and measures the fraction of the LO contribution to M_π^2, is essentially not constrained, even though values close to 2 are slightly disfavoured. If we consider πK scattering only, r and $Y(3)$ are essentially not constrained. Flat CLs are observed for $X(3)$ and $Z(3)$, with a steep decrease respectively for 0.83 and 1. Finally, if we combine both pieces of information, intermediate values of r are clearly favoured (between 20 and 25), in agreement with the information contained in $\pi\pi$ and πK scattering data. Low values of $X(3)$ and $Y(3)$ are preferred, whereas the CL for $Z(3)$ peaks around 0.8. We see that the combination of the two data sets provides more stringent constraints on the various theoretical parameters of interest (this issue is discussed in more detail in Appendix D), even though these results have still a limited statistical significance.

We recall that the frequentist method given here provides an upper bound on the confidence level (CL) for the

optimal set of theoretical parameters assuming $T_i = t_i$ [17]. In the ideal case, we would expect the CL to peak in a very limited interval of t_i, providing the "true" value of the corresponding theoretical parameter. In practice, we see that the chosen set of data is not accurate enough to provide very stringent constraints on the theoretical parameters. In such a case, the CL profiles can be exploited to extract a confidence interval, say at 68% CL, i.e. a range of values so that the probability that the range contains the true value of the parameter is 68%. This can be obtained by determining the region of parameter space in which the CL curve lies above 0.32 [18, 19].

From the CL profiles obtained from the combined analysis of $\pi\pi$ and πK scattering, we obtain the following confidence intervals at 68% CL:

$$r \geq 14.8\,, \quad X(3) \leq 0.83\,, \qquad (70)$$
$$Y(3) \leq 1.1\,, \quad 0.18 \leq Z(3) \leq 1 \quad [68\%\mathrm{CL}]\,.$$

The values for L_1, L_2 and L_3 can also be determined in each case, and the corresponding confidence intervals are collected in Table 1.

As a cross-check, we have also studied the case where the higher-order direct remainders are removed, i.e. (43)–(45) are set to zero. The corresponding CLs are sharper, but very similar in shape to those presented here. Therefore, the polynomial terms modeling higher order contributions tend to push CLs towards 1, but the qualitative features shown in Figs. 1 and 2 stem mainly from the matching of LO and NLO terms of the ReχPT expansion to experimental information.

The scenario mildly favoured from the matching of both $\pi\pi$ and πK scatterings would correspond to a value of $r = m_s/m$ quite close to the canonical value $r = 25$. However, we emphasise that this agreement is rather coincidental: the latter value comes from the (perturbative) reexpression of M_K^2/M_π^2 in terms of r, assuming that the chiral expansions of the two squared masses converge quickly. This assumption is not supported by our results for the quark condensate (or X), which exhibits some suppression when one moves from the $N_f = 2$ chiral limit to the $N_f = 3$ one, i.e., when m_s decreases from its physical value down to zero. On the other hand, the pion decay constant (or Z) seems quite stable from $N_f = 2$ to $N_f = 3$; see (6)–(7). If our results are confirmed by further experimental data, we expect the usual treatment of the $N_f = 3$ chiral expansions to yield unstable expansions, with significant numerical competition among terms of different orders in the chiral counting.

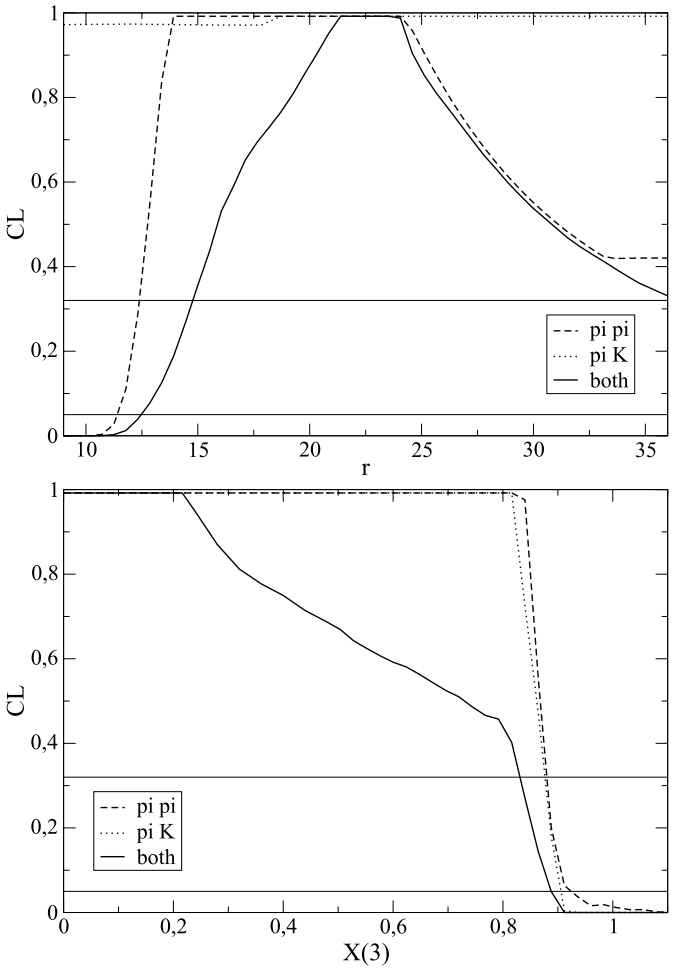

Fig. 1. CL profiles for $r = m_s/m$ (*top*) and $X(3) = 2m\Sigma(3)/(F_\pi^2 M_\pi^2)$ (*bottom*). The *dashed line* corresponds to experimental information on $\pi\pi$ scattering, the *dotted line* to πK scattering, and the *solid line* to the combination of both sets. The *two horizontal lines* indicate the confidence intervals at 68 and 95% CL

Such a situation is reminiscent of a scenario proposed some time ago concerning the N_f-dependence of the chiral structure of QCD vacuum [1, 39, 40]. The quark condensate

Table 1. Derivative chiral couplings $L^{\mathrm{r}}_{1,2,3}(\mu)$ at $\mu = 0.77$ GeV obtained in our approach. The confidence intervals correspond to a 68% CL. "nd" means that the corresponding CL is flat over the whole range imposed by the theoretical likelihood, and thus the coupling is not determined. Also shown are results obtained assuming small vacuum fluctuations of $s\bar{s}$ pairs: [14] analysed subthreshold πK parameters from the Roy–Steiner equations at order p^4 (col. 5), whereas [43–45] performed fits to the Kl_4 form factors using chiral expansions at order p^4 (col. 6) as well as p^6 (col. 7)

	$\pi\pi$ data	πK data	$\pi\pi$ and πK	Roy–Steiner $O(p^4)$	Kl_4, $O(p^4)$	Kl_4, $O(p^6)$
$10^3\, L_1$	$[-8.1, 5.6]$	$[-4.4, 4.1]$	$[-2.1, 2.2]$	1.05 ± 0.12	0.46 ± 0.24	0.53 ± 0.25
$10^3\, L_2$	$[0.2, 2.4]$	nd	$[0, 3.0]$	1.32 ± 0.03	1.49 ± 0.23	0.71 ± 0.27
$10^3\, L_3$	nd	nd	$[-7.8, 3.4]$	-4.53 ± 0.14	-3.18 ± 0.85	-2.72 ± 1.12

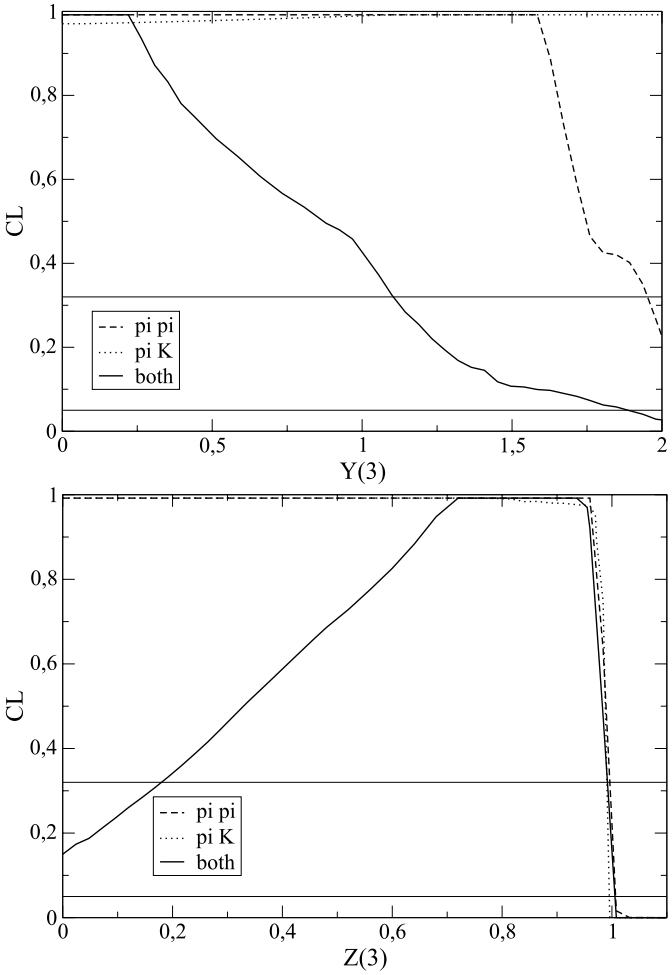

Fig. 2. CL profiles for $Y(3) = 2mB_0/M_\pi^2$ (*top*) and $Z(3) = F_0^2/F_\pi^2$ (*bottom*). The *dashed line* corresponds to experimental information on $\pi\pi$ scattering, the *dotted line* to πK scattering, and the *solid line* to the combination of both sets. The *two horizontal lines* indicate the confidence intervals at 68 and 95% CL

$\Sigma(N_f)$ and the decay constant $F(N_f)$ depend on the way small eigenvalues of the Dirac operator accumulate around zero in the thermodynamic limit. It was conjectured that the two order parameters could decrease at a different rate when the number of massless flavours N_f increases: the quark condensate would vanish first, followed later by the vanishing of the decay constant related to the restoration of chiral symmetry. The trend of our results for $N_f = 3$ order parameters, compared to $N_f = 2$ results, could fit such a scenario, but more data should be included in the analysis before we reach statistically significant CLs for the various theoretical parameters analysed here.

5.2 Comparison with some earlier works

5.2.1 $\pi\pi$ scattering

For$\pi\pi$ scattering, it is interesting to compare our results with [16], which shares some ideas and issues with the present paper. This work differs on three points from [16]: we include πK scattering in our analysis, we choose as observables the scattering amplitudes in subthreshold regions rather than the subtraction constants involved in dispersive representations, and we perform the statistical analysis in a frequentist framework rather than in a Bayesian one.

We observe the same qualitative features in both analyses. As expected, low values of r are strongly disfavoured. Indeed, the analysis of currently available data on $\pi\pi$ scattering [5] provides a value of $X(2)$; see (6). As illustrated in Fig. 1 of [1], $X(2)$ is related to r through the pion and kaon mass and decay constant identities, (15)–(18): the value of $X(2)$ from [5] favours the same range for the quark mass ratio as the upper plot in Fig. 1. On the other hand, we find that $X(3)$ and $Z(3)$ are only constrained through an upper bound, in numerical agreement with the paramagnetic inequalities $X(3) \leq X(2)$ and $Z(3) \leq Z(2)$.

This agreement is particularly gratifying since the method of analysis of the present work does not require computing any $N_f = 2$ chiral order parameters or related subtraction constants like [5, 16]. Moreover, one can see an improvement compared to the latter references, thanks to the frequentist approach chosen here. In [16], it was difficult to disentangle the effect of the data from that of the Bayesian priors inside a posterior PDF: the so-called "reference profiles" (PDFs from priors but no data) had to be compared to the posterior PDFs (PDFs from priors and data) to judge the impact of $\pi\pi$ data. In the present paper, this intricate procedure and the arbitrariness induced by Bayesian priors are avoided: it is clearly seen that $\pi\pi$ data constrain $X(3)$ and $Z(3)$ only through the values of $X(2)$ and $Z(2)$ and the corresponding paramagnetic upper bounds.

5.2.2 πK scattering

For πK scattering, we can compare our results with [14], where the solutions of the Roy–Steiner dispersion relations were used to reconstruct the amplitudes in the subthreshold region. These amplitudes were expanded around the point $s = u$, $t = 0$, and the coefficients of the polynomials, C_{ij}^+ and C_{ij}^-, were matched with their NLO chiral expansions in order to determine some $O(p^4)$ LECs. This led to the determination of L_1, L_2 and L_3 recalled in the previous section, and to a value of L_4 suggesting a significant suppression of $Z(3)$. The value of L_6, though affected by large uncertainties, indicated also a suppression of $X(3)$, stronger than that of $Z(3)$:

$$[14]: \; L_4^{\mathrm{r}}(M_\rho) = (0.53 \pm 0.39) \times 10^{-3}, \qquad (71)$$
$$[2L_6^{\mathrm{r}} + L_8^{\mathrm{r}}](M_\rho) = (3.66 \pm 1.52) \times 10^{-3}.$$

Using (34) and the other results of Sect. 3.1 in [16], and taking $L_8^{\mathrm{r}}(M_\rho) = (0.9 \pm 0.3) \times 10^{-3}$ [13] we can convert these results into the parameters of interest: following these results, $X(3)$ would be between 0.15 and 0.41, $Z(3)$ between 0.14 and 0.92, and $Y(3)$ between 0.44 and 1.05. Obviously, the low values of $X(3)$ and $Z(3)$ indicate that the values obtained in [14], relying on the assumption of small vacuum fluctuations and on $X(3)$ and $Z(3)$ close to 1, should be reassessed relaxing this hypothesis.

If our results for the combined $\pi\pi$ and πK data point towards a similar pattern, our analysis of the πK data alone provides weaker constraints than that of [14]. At least two different reasons lead us to weaker constraints. First, we have explicitly take into account the presence of NNLO contributions that were neglected in the $O(p^4)$ analysis of [14] and that may affect significantly the energy-dependent part of the amplitudes. Secondly, the analysis in [14] assumes explicitly the smallness of vacuum fluctuations: once we drop this assumption, a smaller value of L_4 (and thus a value of $Z(3)$ close to 1) can be compensated by the variation of other parameters, such as the quark mass ratio r. These two phenomena may explain the weaker constraints observed in our analysis.

5.2.3 Combined analyses

For the combined analysis of $\pi\pi$ and πK scatterings, we can compare our results with [28, 29]. The authors of these references took an approach different from ours, computing NNLO chiral expansions to $\pi\pi$ and πK scattering amplitudes, and matching with results on $\pi\pi$ scattering (scattering lengths) and πK scattering (scattering lengths and subthreshold expansion coefficients), supplemented with information on $K_{\ell 4}$ form factors. In agreement with the one-loop framework of [13], these two-loop computations assume a numerical dominance of LO contributions and a quick convergence of $N_f = 3$ chiral expansions.

In previous studies in this NNLO framework [30], the authors performed fits to pseudoscalar masses and decay constants [31, 32], $K_{\ell 3}$ decays [33], and scalar form factors [27]. In each case, the values of the Zweig rule suppressed $O(p^4)$ LECs L_4 and L_6 had to be fixed by hand: fits of similarity quality could be obtained with values of these two constants corresponding either to small or large vacuum fluctuations of $s\bar{s}$ pairs. For scalar form factors, values of L_4 and L_6 larger than conventionally assumed led to an improvement in the convergence of observables (fits A, B and C compared to fit 10 in Table 2 of [27]).

In the case of [28, 29], the authors analysed $\pi\pi$ and πK scattering amplitudes in the same NNLO framework. The fits were not able to reproduce some observables, in particular among πK subthreshold coefficients. A particular subset of subthreshold coefficients and scattering lengths led to $L_4^{\mathrm{r}}(M_\rho) \simeq 0.2 \times 10^{-3}$ and $L_6(M_\rho)$ negative. Such values correspond to F_0 rather small compared to F_π, with a rather unsatisfying convergence of some observables: for instance, the pion mass exhibits instabilities in its chiral expansion [30]. It proves difficult to draw a fully consistent picture for the structure of the QCD vacuum in the $N_f = 3$ chiral limit from these results.

Some of the problems encountered in [28, 29] were reassessed in [41]; in particular the determination of NNLO LECs. Following [42], the many $O(p^6)$ LECs are often estimated using resonance saturation. In [41], the specific resonance Lagrangian used in [28, 29] was shown to provide values for vector-dominated LECs rather far away from the expectations based on πK dispersion relations, but other resonance Lagrangians failed also to repro duce the same results. Therefore, one may wonder whether the problems of convergence seen in [30] could stem from two different sources. The first one consists in the use of resonance saturation to fix $O(p^6)$ counterterms, which is already delicate in vector channels and certainly questionable in the scalar sector. The second one is the observed slow convergence of chiral expansions, which contradicts the starting assumptions of the NNLO analysis. A comparison of ReχPT expansions with the NNLO formulae in [28, 29] should highlight how large values of the $O(p^4)$ LECs L_4 and L_6 might destabilise NNLO expansions and how the explicit resummation of vacuum fluctuations of our work echoes in the perturbative expansion adopted in the latter references.

5.2.4 Lattice

Other interesting developments are awaited from lattice simulations. The effects presented in this paper are related to strange sea quarks, and they can be tackled only with $(2+1)$ dynamical fermions with light masses. Unfortunately, fermions with interesting chiral properties (Wilson, Ginsparg–Wilson, twisted mass) [9–12] are still with at most two dynamical flavours. On the other hand, staggered fermions [46] have been exploited for simulations with $(2+1)$ dynamical quarks, but their use is under much debate [47–51]. The presence of the fourth root of the fermion determinant yields non-localities, which are not understood yet: at best, recovering QCD requires taking the various continuum limits in a very careful way.

A staggered version of chiral perturbation theory [52] has been developed to extract chiral LECs from the pseudoscalar spectrum. It attempts to reproduce the fourth-rooting of the fermion determinant and includes many other effects (lattice spacing, finite-volume effects, taste-breaking terms), leading to a number of LECs much larger than in continuum unstaggered χPT. The hope is that the LECs common to both theories should be identical because QCD ought to be recovered as a limit of lattice QCD with fourth-rooted staggered fermions. In practice [46], chiral fits to staggered data on the pseudoscalar spectrum must include a large number of parameters and thus are highly non-trivial. Mixed actions with domain-wall valence quarks and staggered sea quarks have also been considered to reduce the number of LECs involved in the associated chiral Lagrangian at the price of losing unitarity in addition to locality [53–55].

Bearing all these remarks in mind, we can focus on the following staggered values:

$$\begin{aligned} [46]:\ r &= 27.2(4)\,, \\ [2L_6^{\mathrm{r}} - L_4^{\mathrm{r}}](M_\eta) &= 0.5(1)(2) \times 10^{-3}\,, \\ L_4^{\mathrm{r}}(M_\eta) &= 0.1(2)(2) \times 10^{-3}\,. \end{aligned} \tag{72}$$

Combining the errors in quadrature and using (34) and the other results of Sect. 3.1 in [16], we can convert these results into the parameters of interest: following these lattice results, $X(3)$ would be between 0.55 and 0.95, $Z(3)$ between 0.57 and 1.04, and $Y(3)$ between 0.67 and 1.08; values that are not in striking disagreement with our results. Obviously, if the values of $X(3)$ and $Z(3)$ are on the

smaller end of these ranges, i.e., if L_6 and L_4 are in the upper end of the range in [46], the assumption of small vacuum fluctuations is not correct, and the extraction of the LECs by means of staggered χPT should be reassessed more carefully.

As an alternative to such tests, which rely strongly on the usual treatment of chiral series, we proposed a lattice test of the size of $s\bar{s}$ vacuum fluctuations based on ReχPT in [56]. We considered simulations with $(2+1)$ flavours, with a strange quark mass at its physical value, but the two u,d light quarks with identical masses $\tilde{m}$ larger than their physical values m and smaller than m_s. The larger values of the u,d masses enhanced the impact of the vacuum fluctuations encoded in L_4 and L_6 on observables such as the masses and decay constants of pions and kaons. This led to a difference in the curvatures of F_P^2 and $F_P^2 M_P^2$ ($P=\pi,K$) as functions of $q=\tilde{m}/m_s$, depending on the size of $X(3)$ and $Z(3)$. The effect was less pronounced in the case of M_P^2, obtained as the ratio of the two former observables, leading to a fairly linear behaviour as a function of q.

In the same reference, we proposed a test of the size of $X(3)$ on the lattice from the pion and kaon spectrum, by considering the dependence on q of the ratios:

$$R_\pi = \frac{\tilde{F}_\pi^2 \tilde{M}_\pi^2}{q F_\pi^2 M_\pi^2}\,, \qquad R_K = \frac{2\tilde{F}_K^2 \tilde{M}_K^2}{(q+1) F_K^2 M_K^2}\,, \tag{73}$$

where $\tilde{F}_\pi^2$ and $\tilde{M}_\pi^2$ denote quantities computed on the lattice with u,d quarks of mass $\tilde{m}$. We assessed the leading finite-volume effects to conclude that large volumes (of sides around 2.5 fm) were required to tame these effects.

In any case, more dedicated studies on $(2+1)$ fermions with different actions, lattice spacings and volumes will be required in order to draw definite conclusions from lattice simulations on the structure of the $N_f=3$ chiral vacuum.

6 Conclusion

Vacuum fluctuations of $s\bar{s}$ pairs can induce significant differences in the pattern of chiral symmetry breaking between the two conceivable chiral limits: $N_f=2$ ($m_u=m_d=0$ but m_s kept at its physical values) and $N_f=3$ ($m_u=m_d=m_s=0$). These fluctuations might lead to a paramagnetic suppression of the two main chiral order parameters in the $N_f=3$ chiral limit, the quark condensate and the pseudoscalar decay constant, compared to their $N_f=2$ counterparts [1, 15]. Then, we would observe numerical competition between leading-order (LO) and next-to-leading-order (NLO) contributions in the chiral series, through the two $O(p^4)$ LECs L_4 and L_6 related to the violation of the Zweig rule in the scalar sector.

In order to shed light on the size of these fluctuations, we developed and modified the framework sketched in [16]: resummed chiral perturbation theory or ReχPT. We applied it to our current knowledge of low-energy $\pi\pi$ and πK scatterings. First, we recalled and detailed our treatment of one-loop chiral series in the case of large vacuum fluctuations: only a subset of "good" observables is assumed to converge globally (so that NNLO contributions are much smaller than the sum of LO and NLO contributions), the chiral series must be treated in a particular way to derive bare expansions and resum the effects of vacuum fluctuations, while NNLO remainders are introduced to keep track of higher-order contributions. Then, in this resummed framework, called ReχPT, we determined the one-loop expansions for $\pi\pi$ and πK scattering amplitudes. Relying on our current experimental knowledge, we exploited solutions of the Roy and Roy–Steiner equations within dispersive representations to determine the values of the amplitudes in subthreshold (unphysical) regions where chiral expansions should converge.

The two representations of the scattering amplitudes were matched in a frequentist approach (inspired by Rfit [17]). The output of this analysis are marginal CL curves, providing an upper bound on the confidence level (CL) for the optimal set of theoretical parameters at fixed $T_i=t_i$: the CL value is the probability that a new series of measurements will agree with the most favourable set of theoretical parameters (at $T_i=t_i$) in a worse way than the experimental results actually used in the analysis [18, 19].

Unfortunately, the marginal CL profiles do not provide sharp peaks and thus stringent constraints on the theoretical parameters at a statistically significant level. However, our results point towards some favoured regions of parameter space; see Figs. 1 and 2. If only $\pi\pi$ scattering is included, the results obtained in earlier works [16] are recovered: small values of r are disfavoured, whereas $X(3)$ and $Z(3)$ are only constrained to remain below their $N_f=2$ counterpart due to paramagnetic inequalities; see (5). πK scattering alone does not constrain strongly the various theoretical parameters, apart from setting bounds on $X(3)$ and $Z(3)$. The combination of the two pieces of information proves more interesting: the CL profile for r peaks around 23, low values of $X(3)$ are preferred, whereas the CL for $Z(3)$ exhibits a broad peak around 0.8.

From the CL curves obtained from the combined analysis of $\pi\pi$ and πK scattering, we obtain the following confidence intervals at 68% CL:

$$\begin{aligned} r \geq 14.8\,, \quad X(3) \leq 0.83\,, \\ Y(3) \leq 1.1\,, \quad 0.18 \leq Z(3) \leq 1 \quad [68\%\text{CL}]\,, \end{aligned} \tag{74}$$

corresponding to the regions of parameter space where the marginal CL profiles lie above 0.32 [18, 19].

The pattern of marginal CL profiles is consistent with the scenario of significant vacuum fluctuations of $s\bar{s}$ pairs. It reminds one of the interesting possibility that the decrease of order parameters from $N_f=2$ massless flavours to $N_f=3$ is steeper in the case of the pseudoscalar decay constant $F^2(N_f)$ than for the quark condensate $\Sigma(N_f)$.

The present analysis constitutes a first attempt to analyse data with a limited statistical significance, and it relies strongly on the experimental results gathered on $\pi\pi$ and πK scatterings. For $\pi\pi$ scattering, new results are expected from the NA48 Collaboration on $K_{\ell 4}$ decays [8] and on the cusp in $K\to 3\pi$ [57–61]. For πK scattering, we hope to obtain more precise information from $D_{\ell 4}$ decays [62–65] and $\tau\to K\pi\nu_\tau$ decays [66–69]. In addition, lattice studies could soon provide results for three light

flavours with well-controlled actions in the chiral regime. These new high-accuracy data should shed some more light on the chiral structure of QCD vacuum and, in particular, on its dependence on the number of massless flavours and the role played by the vacuum fluctuations of $s\bar{s}$ pairs.

Acknowledgements. It is a pleasure to thank L. Girlanda, J.J. Sanz-Cillero and J. Stern for collaboration in the early stages of this work, D. Becirevic and B. Moussallam for fruitful discussions and N.H. Fuchs for many useful suggestions on the manuscript. This work was supported in part by the EU Contract No. MRTN-CT-2006-035482, "FLAVIAnet".

Appendix A: One-loop bare expansions of scattering amplitudes

A.1 $\pi\pi$ scattering amplitude

Following the prescription in Sect. 2.2 we obtain, for instance from [23],

$$\begin{aligned}
F_\pi^4 A_{\pi\pi} = {} & \frac{2}{3}mB_0F_0^2 + F_0^2\left(s-\frac{4}{3}M_\pi^2\right) \\
& + \mu_\pi F_0^2\left[-4\left(s-\frac{4}{3}M_\pi^2\right)-2B_0m\right] \\
& + \mu_K F_0^2\left[-2\left(s-\frac{4}{3}M_\pi^2\right)-\frac{4}{3}B_0m\right] \\
& - \frac{2}{9}\mu_\eta F_0^2 B_0 m \\
& + 16B_0mL_4^{\rm r}\left[\left(s-\frac{4}{3}M_\pi^2\right)(r+4)-\frac{4}{3}M_\pi^2\right] \\
& + 32B_0mL_5^{\rm r}\left(s-\frac{5}{3}M_\pi^2\right) \\
& + \frac{64}{3}B_0^2m^2L_6^{\rm r}(r+8)+\frac{256}{3}B_0^2m^2L_8^{\rm r} \\
& + 4\left(2L_1^{\rm r}+L_3^{\rm r}\right)\left(s-2M_\pi^2\right)^2 \\
& + 4L_2^{\rm r}\left[\left(t-2M_\pi^2\right)^2+\left(u-2M_\pi^2\right)^2\right] \\
& + \frac{1}{2}\left[\left(s-2M_\pi^2\right)^2+8mB_0\left(s-2M_\pi^2\right)+12B_0^2m^2\right] \\
& \times J_{\pi\pi}^{\rm r}(s) \\
& + \frac{1}{4}\left[\left(t-2M_\pi^2\right)^2 J_{\pi\pi}^{\rm r}(t)+\left(u-2M_\pi^2\right)^2 J_{\pi\pi}^{\rm r}(u)\right] \\
& + \frac{1}{8}\left[\left(s-2M_\pi^2\right)^2+8mB_0\left(s-2M_\pi^2\right)+16B_0^2m^2\right] \\
& \times J_{KK}^{\rm r}(s)+\frac{2}{9}B_0^2m^2J_{\eta\eta}^{\rm r}(s) \\
& + \frac{1}{2}[(s-u)t\left(2M_{\pi\pi}^{\rm r}+M_{KK}^{\rm r}\right)(t) \\
& + (s-t)u\left(2M_{\pi\pi}^{\rm r}+M_{KK}^{\rm r}\right)(u)]\,,
\end{aligned} \tag{A.1}$$

where $\overset{\circ}{M}{}_P^2$ denotes the leading-order pseudoscalar squared mass of the Goldstone boson P and the tadpole logarithm is

$$\mu_P = \frac{\overset{\circ}{M}{}_P^2}{32\pi^2F_0^2}\log\frac{M_P^2}{\mu^2}\,. \tag{A.2}$$

We recast the amplitude in the following form:

$$\begin{aligned}
F_\pi^4 A_{\pi\pi} = {} & \mathcal{A} + \left(s-\frac{4}{3}M_\pi^2\right)\times\mathcal{B} \\
& + 4\left(2L_1^{\rm r}+L_3\right)\left(s-2M_\pi^2\right)^2 \\
& + 4L_2^{\rm r}\left[\left(t-2M_\pi^2\right)^2+\left(u-2M_\pi^2\right)^2\right] \\
& + \frac{1}{2}\left[\left(s-2M_\pi^2\right)^2+8mB_0\left(s-2M_\pi^2\right)+12m^2B_0^2\right] \\
& \times J_{\pi\pi}^{\rm r}(s) \\
& + \frac{1}{4}\left[\left(t-2M_\pi^2\right)^2 J_{\pi\pi}^{\rm r}(t)+\left(u-2M_\pi^2\right)^2 J_{\pi\pi}^{\rm r}(u)\right] \\
& + \frac{1}{8}\left[\left(s-2M_\pi^2\right)^2+8mB_0\left(s-2M_\pi^2\right)+16m^2B_0^2\right] \\
& \times J_{KK}^{\rm r}(s)+\frac{1}{18}4m^2B_0^2J_{\eta\eta}^{\rm r}(s) \\
& + \frac{1}{2}\left[(s-u)t\times\left(2M_{\pi\pi}^{\rm r}+M_{KK}^{\rm r}\right)(t)\right. \\
& \left.+(s-t)u\times\left(2M_{\pi\pi}^{\rm r}+M_{KK}^{\rm r}\right)(u)\right]\,,
\end{aligned} \tag{A.3}$$

where $\mathcal{A}$ and $\mathcal{B}$ are scale-dependent combinations of LECs:

$$\begin{aligned}
3\times\mathcal{A} = {} & 2mB_0F_0^2+64m^2B_0^2\left[(r+8)L_6^{\rm r}+4L_8^{\rm r}\right] \\
& - 32mB_0M_\pi^2\left[2L_4^{\rm r}+L_5^{\rm r}\right] \\
& - \frac{1}{32\pi^2}4m^2B_0^2\left[3\log\frac{M_\pi^2}{\mu^2}+(r+1)\log\frac{M_K^2}{\mu^2}\right. \\
& \left. + \frac{1}{9}(2r+1)\log\frac{M_\eta^2}{\mu^2}\right]\,,
\end{aligned} \tag{A.4}$$

$$\begin{aligned}
\mathcal{B} = {} & F_0^2+16mB_0\left[(r+4)L_4^{\rm r}+2L_5^{\rm r}\right] \\
& - \frac{1}{32\pi^2}2mB_0\left[4\log\frac{M_\pi^2}{\mu^2}+(r+1)\log\frac{M_K^2}{\mu^2}\right]\,,
\end{aligned} \tag{A.5}$$

which correspond to $F_\pi^2M_\pi^2\alpha_{\pi\pi}^{\rm r}/3$ and $\mathcal{B}$ to $F_\pi^2\beta_{\pi\pi}^{\rm r}$, respectively, as defined in [23].

In the above expressions, we have replaced the bare masses by the physical masses in the (tadpole) logs and in the loop functions $J^{\rm r}$ and $M^{\rm r}$. One can check explicitly that there is no μ-dependence in the above expression of the amplitude: for each polynomial in $s-2M_\pi^2, t-2M_\pi^2, u-2M_\pi^2$, the dependence of the LECs on the renormalisation scale μ cancels that of $J^{\rm r}$ and $M^{\rm r}$.

A.2 πK scattering amplitude

We recall the expression obtained in [35] for the $I=3/2$ amplitude:

$$\begin{aligned}
& F_\pi^2F_K^2F_{\pi K}^{3/2} \\
& = \frac{F_0^2}{6}\left[2M_\pi^2+2M_K^2+\overset{\circ}{M}{}_\pi^2+\overset{\circ}{M}{}_K^2-3s\right.
\end{aligned}$$

$$
\begin{aligned}
&+\frac{\mu_\pi}{8}\left[66s-34M_\pi^2-54M_K^2-15\,\mathring{M}_\pi^2-21\,\mathring{M}_K^2\right]\\
&+\frac{\mu_K}{4}\left[30s-22M_\pi^2-18M_K^2-11\,\mathring{M}_\pi^2-9\,\mathring{M}_K^2\right]\\
&+\frac{\mu_\eta}{24}\left[54s-54M_\pi^2-18M_K^2-17\,\mathring{M}_\pi^2-11\,\mathring{M}_K^2\right]\\
&+8L_1^{\mathrm{r}}\left(t-2M_\pi^2\right)\left(t-2M_K^2\right)\\
&+4L_2^{\mathrm{r}}\left[\left(s-M_\pi^2-M_K^2\right)^2+\left(u-M_\pi^2-M_K^2\right)^2\right]\\
&+2L_3\left[\left(u-M_\pi^2-M_K^2\right)^2+\left(t-2M_\pi^2\right)\left(t-2M_K^2\right)\right]\\
&+8L_4^{\mathrm{r}}\left[\mathring{M}_\pi^2\left(t-\frac{1}{2}s+\frac{1}{3}M_\pi^2-\frac{5}{3}M_K^2\right)\right.\\
&\left.+\,\mathring{M}_K^2\left(t-s-\frac{4}{3}M_\pi^2+\frac{2}{3}M_K^2\right)\right]\\
&+\frac{4}{3}L_5^{\mathrm{r}}\left[\mathring{M}_\pi^2\left(2M_\pi^2-3s\right)+\mathring{M}_K^2\left(2M_K^2-3s\right)\right]\\
&+\frac{8}{3}L_6^{\mathrm{r}}\left[\mathring{M}_\pi^4+15\,\mathring{M}_\pi^2\mathring{M}_K^2+2\,\mathring{M}_K^4\right]\\
&+\frac{8}{3}L_8^{\mathrm{r}}\left[\mathring{M}_\pi^4+6\,\mathring{M}_\pi^2\mathring{M}_K^2+\mathring{M}_K^4\right]\\
&+\frac{t}{2}\left(u-s\right)\left[M_{\pi\pi}^{\mathrm{r}}\left(t\right)+\frac{1}{2}M_{KK}^{\mathrm{r}}\left(t\right)\right]\\
&+\frac{3}{8}\left\{\left(s-t\right)\left[L_{\pi K}\left(u\right)-uM_{\pi K}^{\mathrm{r}}\left(u\right)\right]\right.\\
&\left.+\left(M_K^2-M_\pi^2\right)^2M_{\pi K}^{\mathrm{r}}\left(u\right)\right\}\\
&+\frac{3}{8}\left\{\left(s-t\right)\left[L_{K\eta}\left(u\right)-uM_{K\eta}^{\mathrm{r}}\left(u\right)\right]\right.\\
&\left.+\left(M_K^2-M_\pi^2\right)^2M_{K\eta}^{\mathrm{r}}\left(u\right)\right\}\\
&+\frac{1}{8}\left(M_K^2-M_\pi^2\right)K_{\pi K}\left(u\right)\\
&\times\left[5\left(u-M_\pi^2-M_K^2\right)+3\,\mathring{M}_\pi^2+3\,\mathring{M}_K^2\right]\\
&+\frac{1}{8}\left(M_K^2-M_\pi^2\right)K_{K\eta}\left(u\right)\\
&\times\left[3\left(u-M_\pi^2-M_K^2\right)+\mathring{M}_\pi^2+\mathring{M}_K^2\right]\\
&+\frac{1}{4}J_{\pi K}^{\mathrm{r}}\left(s\right)\left(s-M_\pi^2-M_K^2\right)^2\\
&+\frac{1}{32}J_{\pi K}^{\mathrm{r}}\left(u\right)\left[11\left(u-M_\pi^2-M_K^2\right)^2\right.\\
&+10\left(u-M_\pi^2-M_K^2\right)\left(\mathring{M}_\pi^2+\mathring{M}_K^2\right)\\
&\left.+3\left(\mathring{M}_\pi^2+\mathring{M}_K^2\right)^2\right]\\
&+\frac{1}{32}J_{K\eta}^{\mathrm{r}}\left(u\right)\left[u-M_\pi^2-M_K^2+\frac{1}{3}\left(\mathring{M}_\pi^2+\mathring{M}_K^2\right)\right]^2\\
&+\frac{1}{8}J_{\pi\pi}^{\mathrm{r}}\left(t\right)\left[4M_\pi^2-2t-3\,\mathring{M}_\pi^2\right]\left[2M_K^2-t-2\,\mathring{M}_K^2\right]\\
&+\frac{3}{16}J_{KK}^{\mathrm{r}}\left(t\right)\left[2M_\pi^2-t-2\,\mathring{M}_\pi^2\right]\left[2M_K^2-t-2\,\mathring{M}_K^2\right]\\
&+\frac{1}{8}J_{\eta\eta}^{\mathrm{r}}\left(t\right)\mathring{M}_\pi^2\left[t-2M_K^2+\frac{10}{9}\,\mathring{M}_K^2\right]\Bigg]\,. \qquad \text{(A.6)}
\end{aligned}
$$

This expression is renormalisation-scale independent. In both $\pi\pi$ and πK scattering, the one-loop expressions obtained with the usual treatment of three-flavour χPT [13] are recovered if we treat chiral series perturbatively and neglect the (potentially large) difference between the truncated $O(p^2)$ expressions and the physical values of the pseudoscalar masses and decay constants.

Appendix B: Computation of the amplitudes

The amplitudes are smooth functions of the various experimental inputs. This means in particular that there will be significant correlations among the values of the same scattering amplitude at different points in the Mandelstam plane. We compute these correlations according to the following procedure. Let us call a_k $(k=1\ldots n)$ the parameters describing the variations of the experimental inputs. To each of these parameters is attached an uncertainty (σ_k), and the correlations among them are encoded in a covariance matrix D_{kl}, or equivalently, a reduced covariance matrix $H_{kl}=D_{kl}/(\sigma_k\sigma_l)$. We compute the mean value m_i of the observables x_i's by setting all the parameters a_k to their central value $\bar{a}_k$: $m_i\equiv x_i(\bar{a}_k)$. Then, we vary the parameters one by one (the others being kept at their central value), and we compute each time

$$\Delta_i^k\equiv x_i\left(\bar{a}_k+\frac{\sigma_k}{\rho}\right)-m_i=\frac{\sigma_k}{\rho}\times\frac{\partial x_i}{\partial a_k}+\ldots\,, \qquad \text{(B.1)}$$

where ρ is a large parameter (around 10), and the ellipsis denotes higher derivatives. Once this is done for all the parameters, we compute the covariance matrix for the observables:

$$V_{ij}\equiv\rho^2\sum_{kl}\Delta_i^k\Delta_j^lH_{kl}=\sum_{kl}\frac{\partial x_i}{\partial a_k}\frac{\partial x_j}{\partial a_l}D_{kl}+\ldots \qquad \text{(B.2)}$$

The same procedure was followed in [14] to determine the correlation matrix between the two πK scattering lengths.

For the $\pi\pi$ scattering amplitude, we obtain the following values and errors for the amplitude at the limits of the subthreshold region (s,t,u):

$$\left(2M_\pi^2,M_\pi^2,M_\pi^2\right)\quad A=2.84\pm0.16\,, \qquad \text{(B.3)}$$

$$\left(M_\pi^2/2,3/2M_\pi^2,3/2M_\pi^2\right)\quad A=-1.03\pm0.12\,, \qquad \text{(B.4)}$$

$$\left(M_\pi^2/2,3M_\pi^2,M_\pi^2/2\right)\quad A=-1.08\pm0.11\,. \qquad \text{(B.5)}$$

For πK scattering, we have in a similar way

$$\left(M_K^2, 2M_\pi^2, M_K^2\right) \quad B = 4.09 \pm 0.64, \quad C = 0\,, \tag{B.6}$$

$$\left(M_K^2, 0, M_K^2 + 2M_\pi^2\right) \quad B = 2.96 \pm 0.60\,, \quad C = -0.95 \pm 0.03\,, \tag{B.7}$$

$$\left(M_K^2 + M_\pi^2, 0, M_K^2 + M_\pi^2\right) \quad B = 2.61 \pm 0.60, \quad C = 0\,. \tag{B.8}$$

The zeroes of C are due to its antisymmetry under s–u exchange. Uncertainties are correlated.

Appendix C: Treatment of correlated data

We expect strong correlations among the data points. This is reflected by the fact that the matrix C is nearly degenerate and therefore cannot be inverted easily. In order to treat this problem, one can diagonalize[4] the matrix C:

$$C = UDU^{\mathrm{T}}\,, \quad D = \mathrm{diag}(\lambda_1, \ldots, \lambda_n)\,, \tag{C.1}$$

$$UU^{\mathrm{T}} = U^{\mathrm{T}}U = 1\,, \tag{C.2}$$

which yields the corresponding likelihood:

$$\mathcal{L}(\Delta V) = \exp\left[-\frac{1}{2}\Delta V^T\, C^{-1}\, \Delta V\right] / \sqrt{\det(2\pi C)} \tag{C.3}$$

$$= \exp\left[-\frac{1}{2}\Delta V^{\mathrm{T}} U D^{-1} U^{\mathrm{T}} \Delta V\right] / \sqrt{\det(2\pi C)}\,. \tag{C.4}$$

Let us split the set of eigenvalues in two categories: large eigenvalues of order 1, collected in the diagonal matrix $\tilde{D}$, and almost vanishing eigenvalues, smaller than a cut-off and gathered in the diagonal matrix D_0:

$$D = \tilde{D} + D_0\,, \quad \tilde{C} = U\tilde{D}U^{\mathrm{T}}\,, \quad C_0 = UD_0U^{\mathrm{T}}\,. \tag{C.5}$$

The eigenvalues in D_0 are responsible for the near degeneracy of the matrix. In the corresponding directions, the exponential could be approximated with a Dirac distribution and would yield constraints on NNLO and higher-order remainders. Our approximation by a low-degree polynomial is expected to hold at the level of a few percent: numerically, a perfect agreement between data and experiment occurs already if $\Delta V = O(1\%)$. Therefore, we cannot make much use of eigenvalues of the covariance matrix much smaller than $(1\%)^2 = 10^{-4}$. This leads us to put a limit on the analysis to the subspace where $\tilde{D}$ is non-vanishing and to define on this subspace $D^{-1} \equiv \tilde{D}^{-1}$ (see Chapter 2.6 in [70] for a more detailed discussion on the relationships between singular value decomposition and matrix inversion). We chose to set the limit between small and large eigenvalues of order 10^{-8} (with only a very mild dependence of our results on the exact value of the cut-off).

[4] In practice, we use the singular value decomposition method described in [70], which introduces two different rotation matrices on the left and on the right. This slight modification does not alter the procedure outlined in this section.

Appendix D: Impact of combining $\pi\pi$ and πK data for marginal CL profiles

As shown in Sect. 5.1, the analysis of $\pi\pi$ data in our framework puts a lower bound on r ($r \geq 12$ at 68% CL), and an upper bound on $X(3)$ and $Z(3)$ (below 0.85 and 0.95 respectively). πK scattering does seem to bring only a lower bound on $X(3)$. The combination of these two pieces of information proves to be much more powerful and allows one to extract CL intervals on r, $X(3)$, $Y(3)$ and $Z(3)$. Indeed, we recall that our statistical method, inspired by the Rfit approach [17], consists in the following steps: determine the absolute minimum of χ^2 first, then fix a particular theoretical parameter a (among r, $X(3)$, $Y(3)$, $Z(3)$) and compute the corresponding relative minimum of χ^2, finally extract a CL (actually a P-value [18, 19] from the difference between the two values of χ^2. This amounts to computing

$$\mathrm{CL}[a|\mathrm{data}] = \mathrm{Max}_\mu \mathrm{CL}[a;\mu|\mathrm{data}]\,, \tag{D.1}$$

where μ collects all the remaining theoretical parameters (including L_i and NNLO remainders). Therefore, the CL profiles obtained in our approach correspond to upper bounds on the CLs. In particular, it is enough that one set of theoretical parameters μ yields the same value of χ^2 as the absolute minimum to get $\mathrm{CL}(a) = 1$.

We have many theoretical parameters for the description of the scattering amplitudes: in addition to r, $X(3)$ and $Z(3)$, we have the $O(p^4)$ LECs $L_{1,2,3}$ and (direct and indirect) NNLO remainders. Therefore, it is not particularly surprising that either $\pi\pi$ or πK scattering alone is not enough to simultaneously put constraints on all these parameters: many equivalent situations (with identical χ^2 and thus CL) can be obtained with different sets of theoretical parameters. This degeneracy, in particular for the minimum χ^2, comes from the possibility of compensating a variation in a by a modification of the remaining theoretical parameters μ within the allowed ranges, which tends to yield flat CL profiles when we consider only one amplitude.

This underdetermination of the theoretical parameters – and the resulting degeneracy in CL values – is lifted once several sets of different sources are considered. In the present case, $\pi\pi$ data put constraints on the quark mass ratio r and on some of the $O(p^4)$ derivative couplings. Because of these constraints, the regions of theoretical parameters with identical CLs are reduced, and thus the CL curves associated with πK scattering exhibit more distinctive features.

As an illustration of this phenomenon, we compute the CL for πK data alone with L_1, L_2, L_3 and r fixed to specific values, in order to mimic the interplay between the $\pi\pi$ and πK data in the CL curves. Let us set L_1, L_2 and L_3 to the values corresponding to the absolute minimum of the

χ^2 when both $\pi\pi$ and πK data are considered:

$$\begin{aligned} L_1^{\rm r}(M_\rho) &= -0.31\times 10^{-3}\,,\\ L_2^{\rm r}(M_\rho) &= 2.12\times 10^{-3}\,,\\ L_3^{\rm r}(M_\rho) &= -0.64\times 10^{-3}\,, \end{aligned} \qquad \text{(D.2)}$$

and let us set r equal to the four different values $r = 10, 20, 30, 35$. With these theoretical parameters fixed, we determine CL$[X(3); r, L_{1,2,3}|\pi K]$ and CL$[Z(3); r, L_{1,2,3}|\pi K]$ profiles, which are drawn in Fig. 3. We can see that the CL profiles of $X(3)$ and $Z(3)$ for $r = 20$ are very similar to the solid lines shown in Figs. 1 and 2, corresponding to $CL[X(3)|\pi\pi, \pi K]$ and $CL[Z(3)|\pi\pi, \pi K]$. On the other hand, the curves for $r = 10, 30, 35$ are somewhat broader and flatter.

The CL curves obtained for πK scattering in Figs. 1 and 2 are CL$[X(3)|\pi K]$ and CL$[Z(3)|\pi K]$, which correspond to the envelope of all the CL profiles of the form CL$[X(3); r, L_{1,2,3}|\pi K]$ and CL$[Z(3); r, L_{1,2,3}|\pi K]$ when varying r (and $L_{1,2,3}$). This superposition, dominated by values of r around 35, eventually yields the flat profiles in $X(3)$ and $Z(3)$ observed in Figs. 1 and 2. On the other hand, when we combine $\pi\pi$ and πK scatterings, a value of r around 20 is preferred by the $\pi\pi$ data (together with some ranges for $L_{1,2,3}$). Therefore, the contribution from πK scattering to CL$[X(3)|\pi\pi, \pi K]$ and CL$[Z(3)|\pi\pi, \pi K]$ is close to the CL curve obtained for CL$[X(3); r = 20, L_{1,2,3}|\pi K]$ and CL$[Z(3); r = 20, L_{1,2,3}|\pi K]$, i.e. $r = 20$ in Fig. 3. This phenomenon explains how the information on the theoretical parameters can be hidden in πK scattering but is unveiled once combined with $\pi\pi$ scattering, lifting the degeneracy in the CLs and leading to a sharper determination of $X(3)$ and $Z(3)$.

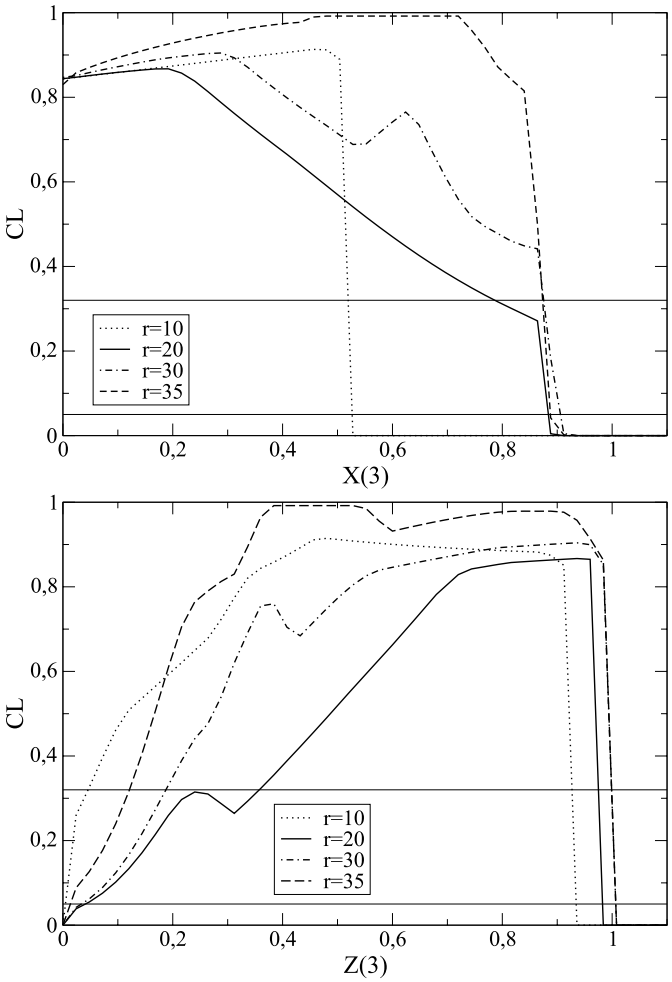

Fig. 3. CL profiles for $X(3) = 2m\Sigma(3)/(F_\pi^2 M_\pi^2$ (*top*) and $Z(3) = F_0^2/F_\pi^2$ (*bottom*), obtained from the combination of the experimental information on $\pi\pi$ and πK scatterings, with L_1, L_2, L_3 set to the values minimizing the complete χ^2 (see text). The *four curves* correspond to the four different (imposed) values of $r = 10, 20, 30, 35$. The *two horizontal lines* indicate the confidence intervals at 68 and 95% CL

References

1. S. Descotes-Genon, L. Girlanda, J. Stern, JHEP **0001**, 041 (2000) [hep-ph/9910537]
2. BNL-E865 Collaboration, S. Pislak et al., Phys. Rev. Lett. **87**, 221 801 (2001) [hep-ex/0106071]
3. BNL-E865 Collaboration, Phys. Rev. D **67**, 072 004 (2003) [hep-ex/0301040]
4. B. Ananthanarayan, G. Colangelo, J. Gasser, H. Leutwyler, Phys. Rep. **353**, 207 (2001) [hep-ph/0005297]
5. S. Descotes-Genon, N.H. Fuchs, L. Girlanda, J. Stern, Eur. Phys. J. C **24**, 469 (2002) [hep-ph/0112088]
6. G. Colangelo, J. Gasser, H. Leutwyler, Phys. Rev. Lett. **86**, 5008 (2001) [hep-ph/0103063]
7. J. Gasser, H. Leutwyler, Ann. Phys. **158**, 142 (1984)
8. NA48 Collaboration, L. Masetti, Talk at the 33rd International Conference on High Energy Physics (ICHEP 06), hep-ex/0610071
9. L. Del Debbio, L. Giusti, M. Luscher, R. Petronzio, N. Tantalo, hep-lat/0610059
10. L. Del Debbio, L. Giusti, M. Luscher, R. Petronzio, N. Tantalo, hep-lat/0701009
11. D. Becirevic, P. Boucaud, V. Lubicz, G. Martinelli, F. Mescia, S. Simula, C. Tarantino, Phys. Rev. D **74**, 034 501 (2006) [hep-lat/0605006]
12. ETM Collaboration, P. Boucaud et al., hep-lat/0701012
13. J. Gasser, H. Leutwyler, Nucl. Phys. B **250**, 465 (1985)
14. P. Büttiker, S. Descotes-Genon, B. Moussallam, Eur. Phys. J. C **33**, 409 (2004) [hep-ph/0310283]
15. S. Descotes-Genon, L. Girlanda, J. Stern, Eur. Phys. J. C **27**, 115 (2003) [hep-ph/0207337]
16. S. Descotes-Genon, N.H. Fuchs, L. Girlanda, J. Stern, Eur. Phys. J. C **34**, 201 (2004) [hep-ph/0311120]
17. A. Hocker, H. Lacker, S. Laplace, F. Le Diberder, Eur. Phys. J. C **21**, 225 (2001) [hep-ph/0104062]
18. W.J. Metzger, Statistical Methods in Data Analysis, http://www.hef.kun.nl/∼wes/stat_course/statist.pdf
19. F. James, Statistical Methods in Experimental Physics, (World Scientific, Singapore, 2006)
20. N.H. Fuchs, H. Sazdjian, J. Stern, Phys. Lett. B **238**, 380 (1990)
21. N.H. Fuchs, Phys. Lett. B **269**, 183 (1991)
22. N.H. Fuchs, Phys. Rev. D **47**, 3814 (1993) [hep-ph/9301244]

23. M. Knecht, B. Moussallam, J. Stern, N.H. Fuchs, Nucl. Phys. B **457**, 513 (1995) [hep-ph/9507319]
24. B. Moussallam, Eur. Phys. J. C **14**, 111 (2000) [hep-ph/9909292]
25. B. Moussallam, JHEP **0008**, 005 (2000) [hep-ph/0005245]
26. S. Descotes-Genon, JHEP **0103**, 002 (2001) [hep-ph/0012221]
27. J. Bijnens, P. Dhonte, JHEP **0310**, 061 (2003) [hep-ph/0307044]
28. J. Bijnens, P. Dhonte, P. Talavera, JHEP **0401**, 050 (2004) [hep-ph/0401039]
29. J. Bijnens, P. Dhonte, P. Talavera, JHEP **0405**, 036 (2004) [hep-ph/0404150]
30. J. Bijnens, Prog. Part. Nucl. Phys. **58**, 521 (2007) [hep-ph/0604043]
31. G. Amoros, J. Bijnens, P. Talavera, Nucl. Phys. B **568**, 319 (2000) [hep-ph/9907264]
32. G. Amoros, Nucl. Phys. B **602**, 87 (2001) [hep-ph/0101127]
33. J. Bijnens, P. Talavera, Nucl. Phys. B **669**, 341 (2003) [hep-ph/0303103]
34. S. Descotes-Genon, J. Stern, Phys. Lett. B **488**, 274 (2000) [hep-ph/0007082]
35. V. Bernard, N. Kaiser, U.G. Meissner, Phys. Rev. D **43**, 2757 (1991)
36. A. Manohar, H. Georgi, Nucl. Phys. B **234**, 189 (1984)
37. H. Georgi, Phys. Lett. B **298**, 187 (1993) [hep-ph/9207278]
38. CKMfitter Group, J. Charles et al., Eur. Phys. J. C **41**, 1 (2005) [hep-ph/0406184]
39. J. Stern, hep-ph/9801282
40. S. Descotes-Genon, J. Stern, Phys. Rev. D **62**, 054011 (2000) [hep-ph/9912234]
41. K. Kampf, B. Moussallam, Eur. Phys. J. C **47**, 723 (2006) [hep-ph/0604125]
42. G. Ecker, J. Gasser, A. Pich, E. de Rafael, Nucl. Phys. B **321**, 311 (1989)
43. G. Amoros, J. Bijnens, P. Talavera, Phys. Lett. B **480**, 71 (2000) [hep-ph/9912398]
44. G. Amoros, Nucl. Phys. B **585**, 293 (2000) [hep-ph/0003258]
45. G. Amoros, Nucl. Phys. B **598**, 665 (2001) [Erratum]
46. MILC Collaboration, C. Bernard et al., hep-lat/0609053
47. M. Creutz, hep-lat/0603020
48. M. Creutz, hep-lat/0701018
49. C. Bernard, M. Golterman, Y. Shamir, S.R. Sharpe, hep-lat/0603027
50. S. Durr, PoS **LAT2005**, 021 (2006) [hep-lat/0509026]
51. S.R. Sharpe, PoS **LAT2006**, 022 (2006) [hep-lat/0610094]
52. S.R. Sharpe, R.S. Van de Water, Phys. Rev. D **71**, 114505 (2005) [hep-lat/0409018]
53. J.W. Chen, D. O'Connell, R.S. Van de Water, A. Walker-Loud, Phys. Rev. D **73**, 074510 (2006) [hep-lat/0510024]
54. D. O'Connell, hep-lat/0609046
55. J.W. Chen, D. O'Connell, A. Walker-Loud, Phys. Rev. D **75**, 054501 (2007) [hep-lat/0611003]
56. S. Descotes-Genon, Eur. Phys. J. C **40**, 81 (2005) [hep-ph/0410233]
57. NA48/2 Collaboration, J.R. Batley et al., Phys. Lett. B **633**, 173 (2006) [hep-ex/0511056]
58. N. Cabibbo, Phys. Rev. Lett. **93**, 121801 (2004) [hep-ph/0405001]
59. N. Cabibbo, G. Isidori, JHEP **0503**, 021 (2005) [hep-ph/0502130]
60. G. Colangelo, J. Gasser, B. Kubis, A. Rusetsky, Phys. Lett. B **638**, 187 (2006) [hep-ph/0604084]
61. E. Gamiz, J. Prades, I. Scimemi, Eur. Phys. J. C **50**, 405 (2007) [hep-ph/0602023]
62. FOCUS Collaboration, J.M. Link et al., Phys. Lett. B **607**, 67 (2005) [hep-ex/0410067]
63. CLEO Collaboration, M.R. Shepherd et al., Phys. Rev. D **74**, 052001 (2006) [hep-ex/0606010]
64. C.L.Y. Lee, M. Lu, M.B. Wise, Phys. Rev. D **46**, 5040 (1992)
65. B. Ananthanarayan, K. Shivaraj, Phys. Lett. B **628**, 223 (2005) [hep-ph/0508116]
66. ALEPH Collaboration, R. Barate et al., Eur. Phys. J. C **11**, 599 (1999) [hep-ex/9903015]
67. OPAL Collaboration, G. Abbiendi et al., Eur. Phys. J. C **35**, 437 (2004) [hep-ex/0406007]
68. M. Jamin, A. Pich, J. Portoles, Phys. Lett. B **640**, 176 (2006) [hep-ph/0605096]
69. M. Jamin, J.A. Oller, A. Pich, Phys. Rev. D **74**, 074009 (2006) [hep-ph/0605095]
70. W.H. Press, S.A. Teukolsky, W.T. Vetterling, B.P. Flannery, Numerical Recipes – The Art of Scientific Computing (Cambridge University Press, Cambridge, 2007)